for both J-aggregates (red) and monometric forms (green) of JC-10 were measured at Ex/Em = 490/525 nm and 540/590 nm with a Varioskan Flush Multimode Reader (Thermo Fisher Scientific, Waltham, MA).

Isolation of Mitochondria

The cells were lysed by mechanical homogenization using a small pestle, and mitochondrial extraction was performed using a Qproteome Mitochondria Isolation kit (Qiagen), according to the manufacturer's instructions. Liver mitochondria were isolated as described previously with some modifications.[27] In brief, the livers were minced on ice and homogenized by five strokes with a Dounce homogenizer and a tight-fitting pestle in isolation buffer [70 mmol/L sucrose, 1 mmol/L KH_2PO_4, 5 mmol/L HEPES, 220 mmol/L mannitol, 5 mmol/L sodium succinate, and 0.1% bovine serum albumin (BSA), pH 7.4]. The homogenate was centrifuged at 800 × *g* for 5 minutes at 4°C. The supernatant fraction was retained, whereas the pellet was washed with isolation buffer and centrifuged again. The combined supernatant fractions were centrifuged at 1000 × *g* for 15 minutes at 4°C to obtain a crude mitochondrial pellet.

Measurement of ROS

The cellular ROS level was measured by oxidation of the cell-permeable, oxidation-sensitive fluorogenic precursor, *2′,7′*-dihydrodichlorofluorescein diacetate (Molecular Probes Inc., Eugene, OR). Fluorescence was measured using a Varioskan Flush Multimode Reader at 495/535 nm (excitation/emission).

Determination of Glutathione Content

Mitochondrial pellets were measured for total glutathione [reduced glutathione (GSH) + oxidized glutathione (GSSG)] and GSH content using the GSSG/GSH Quantification kit (Dojindo Molecular Technologies, Inc., Kumamoto, Japan). The concentration of GSH was calculated using the following formula:

$$\text{GSH concentration} = \text{Total glutathione concentration} - [\text{GSSG concentration}] \times 2 \quad (1)$$

The liver tissue samples (approximately 50 mg) were minced in ice-cold metaphosphoric acid solution, homogenized, and centrifuged at 3000 × *g* for 10 minutes at 4°C. Lysates from the liver tissue samples and mitochondrial samples (2 mg) were evaluated for the concentration of GSH using the thioester method and a GSH-400 kit (Oxis International Inc., Portland, OR) and for total glutathione content using the glutathione reductase–dinitrothiocyanobenzene recycling assay and the GSH-412 kit (Oxis International Inc.), as described previously.[5]

Immunoblotting

Samples were lysed in radioimmunoprecipitation assay buffer [20 mmol/L Tris-HCl (pH 7.5), 150 mmol/L NaCl, 50 mmol/L NaF, 1 mmol/L Na_3VO_4, 0.1% SDS, and 0.5% Triton X-100], as described previously,[28] supplemented with 1% protease inhibitor mixture (Sigma-Aldrich) and 100 mmol/L phenylmethylsulfonyl fluoride. Cell lysates or mitochondrial pellets were subjected to immunoblot analysis using an iBlot Gel Transfer Device (Invitrogen, Carlsbad, CA). The membranes were incubated with the following primary antibodies: rabbit anti-human LC3 (Novus Biologicals, Littleton, CO), rabbit anti-human p62/SQSTM1 (MBL, Nagoya, Japan), rabbit anti-human Parkin (Cell Signaling Technology, Danvers, MA), mouse anti-human Parkin (Santa Cruz Biotechnology, Inc.), rabbit anti-human p-Parkin (Ser 378; Santa Cruz Biotechnology, Inc.), rabbit anti-human PINK1 (Cell Signaling Technology), mouse anti-human mitochondrial heat shock protein-70 (BioReagents, Golden, CO), mouse anti-human ubiquitin (Santa Cruz Biotechnology, Inc.), goat anti-human voltage-dependent anion-selective channel protein 1 (VDAC1; Santa Cruz Biotechnology, Inc.), monoclonal antisynthetic HCV core peptide (CP11; Institute of Immunology, Ltd), mouse anti-HCV non-structural (NS) 3 protein (Abcam, Cambridge, MA), mouse anti-HCV NS4A (Abcam), mouse anti-HCV NS5A protein (Abcam), and rabbit anti-human β-actin (Cell Signaling Technology).

Electron Microscopy

To address the detail localization of core and Parkin, the cells treated with CCCP for 1 hour were fixed with 4% paraformaldehyde and 1% glutaraldehyde in 0.1 mol/L Millonig's phosphate buffer (pH 7.4) for 30 minutes. The cells were incubated with a mixture of the following primary antibodies in phosphate-buffered saline (PBS) containing 1% BSA and 0.05% sodium azide overnight at 20°C: mouse monoclonal antisynthetic HCV core peptide (Institute of Immunology), rabbit anti-human Parkin (Abcam), and rabbit anti-rat LC3 (Wako Pure Chemical Industries, Ltd, Osaka, Japan). After washing with PBS, the cells were incubated with biotinylated donkey anti-rabbit IgG (Jackson ImmunoResearch Laboratories, Inc., Baltimore Pike, PA) in 1% BSA for 2 hours at 20°C. After washing with PBS, the cells were incubated with Alexa Fluor-488 FluroNanogold-streptavidin (Jackson ImmunoResearch Laboratories, Inc.), indocarbocyanine-labeled donkey anti-mouse IgG (Jackson ImmunoResearch Laboratories, Inc.), and indocarbocyanine-labeled donkey anti-rabbit IgG (Jackson ImmunoResearch Laboratories, Inc.) in 1% BSA for 2 hours at 20°C. After washing with PBS, the cells were incubated with mouse peroxidase–anti-peroxidase complex (Jackson ImmunoResearch Laboratories, Inc.) in PBS for 3 hours at 20°C. The peroxidase reduction was developed with 0.05% diaminobenzidine tetrahydrochloride in 50 mmol/L Tris buffer containing 0.01% hydrogen peroxide for 20 minutes at room temperature. The diameter of the gold immunoparticles was increased using a silver enhancement kit (HQ silver; Nanoprobes, Inc., Yaphank, NY) for 4 minutes at

room temperature. After treatment with 1% osmium and 2% uranyl acetate, the cells were dehydrated in a graded series of ethanol and embedded in Epon-Araldite (OKEN, Tokyo, Japan). Serial ultrathin sections (each 70 nm thick) were examined using an electron microscope (model JEM1400; JEOL, Tokyo, Japan). These immune–electron microscopic methods were generally performed according to our previous study.[29]

Immunofluorescence Microscopy

The cells were fixed, permeabilized, and immunostained with rabbit anti-human Parkin (Abcam), goat anti-human Parkin (Santa Cruz Biotechnology, Inc.), goat anti-human Tom20 (Santa Cruz Biotechnology, Inc.), rabbit anti-rat LC3 (Wako Pure Chemical Industries, Ltd), or mouse monoclonal anti-synthetic HCV core peptide (Institute of Immunology) antibodies, followed by Cy3-conjugated donkey anti-rabbit IgG (Jackson ImmunoResearch Laboratories, Inc.), fluorescein isothiocyanate–conjugated donkey anti-goat IgG (Jackson ImmunoResearch Laboratories, Inc.), or Alexa Fluor 647–conjugated donkey anti-mouse IgG (Jackson ImmunoResearch Laboratories, Inc.). Cell images were captured using a confocal microscope (model LSM700; Zeiss, Jena, Germany) equipped with 488-, 555-, and 639-nm diodes. The images were acquired in a sequential mode using a 63× Plan Apochromat numerical aperture/1.4 oil objective and the appropriate filter combinations. All images were saved as tagged image file format files. The contrast was adjusted using Photoshop version CS5 (Adobe, San Jose, CA), and the images were imported into Illustrator version CS5 (Adobe). Colocalization was assessed with line scans using ImageJ software version 1.46 (NIH, Bethesda, MD).

Coimmunoprecipitation

Coimmunoprecipitation was performed using a Dynabeads Co-Immunoprecipitation Kit (Invitrogen), according to the manufacturer's instructions. Magnetic beads (Dynabeads M-270 Epoxy) were conjugated to anti-VDAC1 (Santa Cruz Biotechnology, Inc.), anti-Parkin (Cell Signaling Technology), anti-ubiquitin (Santa Cruz Biotechnology, Inc.), or anti-p62 (MBL) antibodies by rotating overnight at 37°C. The antibody-Dynabeads complex was then treated with coupling buffer. Beads coupled to anti-VDAC, anti-Parkin, anti-ubiquitin, or anti-p62 were incubated with cell lysates for 30 minutes at 4°C and then washed with coupling buffer. Collected protein complexes were subjected to immunoblot analysis using anti-VDAC, anti-ubiquitin (Santa Cruz Biotechnology, Inc.), and anti-Parkin (Cell Signaling Technology) antibodies to detect coimmunoprecipitated VDAC1, ubiquitin, and Parkin. Immunoblots using anti-Parkin, anti-HCV core (Institute of Immunology), anti-HCV NS3 (Abcam), anti-HCV NS4A (Abcam), or anti-HCV NS5A (Abcam) antibodies were performed to detect the coimmunoprecipitation of Parkin with core, NS3, NS4A, or NS5A protein.

RNA Interference

The siRNA knockdown oligonucleotides were obtained from Invitrogen. JFH1-Huh7 cells and/or Huh7 cells were grown to 50% to 60% confluency and transfected with 100 pmol siRNA oligonucleotides [5′-GGACGCUGUUCCUCGUUAUGAA-GAA-3′ (forward) and 5′-UUCUUCAUAACGAGGAACA-GCGUCC-3′ (reverse)] for PINK1 or siRNA oligonucleotides [5′-UCCAGCUCAAGGAGGUGGUUGCUAA-3′ (forward) and 5′-UUAGCAACCACCUCCUUGAGCUGGA-3′ (reverse)] for Parkin using Lipofectamine 2000 (Invitrogen). The cells were analyzed 72 hours after transfection.

Yeast Two-Hybrid Assay

A Matchmaker Gal4 two-hybrid system 3 (Clontech Laboratories, Inc., Mountain View, CA) was used according to the manufacturer's instructions. *Saccharomyces cerevisiae* Y187, containing an N- or C-terminal fragment cDNA of Parkin as a prey cloned into the Gal4-activation domain vector (pACT2), was allowed to mate with *S. cerevisiae* AH109, which had been transformed with a Gal4 DNA-binding domain vector (pGBKT7) containing the HCV core as bait. In addition, *S. cerevisiae* Y187, with the HCV core as a prey cloned into the Gal4-activation domain vector (pACT2), was allowed to mate with *S. cerevisiae* AH109, which had been transformed with a Gal4 DNA-binding domain vector (pGBKT7) containing N- or C-terminal fragment cDNA of Parkin as bait. To construct the prey and the bait, two regions of the Parkin gene that encoded the N-terminal 215–amino acid residues (1 to 215) and the C-terminal 250–amino acid residues (216 to 465) were amplified using PCR with genomic cDNA, and the HCV core gene was amplified with the HCV-O (genotype *1b*) genomic cDNA.[30] The PCR primers were as follows with the incorporated BamHI and EcoRI sites underlined: Parkin 1 to 215, 5′-GGATCCGCATGATAGTGTTTGTCAGGTT-3′ (forward) and 5′-GAATTCCTAGTGTGCTCCACATTTAA-AGA-3′ (reverse); Parkin 216 to 465, 5′-GGATCCGCCC-CACCTCTGACAAGGAAAC-3′ (forward) and 5′-GAAT-TCCTACACGTCGAACCAGTGGT-3′ (reverse); and HCV core, 5′-GAATTCGCCATGAGCACAAATCCTAAACCT-C-3′ (forward) and 5′-GGATCCTTAAGCGGAAGCTGG-GATGGTCAAA-3′ (reverse).

Real-Time RT-PCR

Total RNA was extracted from frozen liver tissues and cells using the RNeasy mini kit (Qiagen). Total RNA (2 μg) was reverse transcribed to cDNA using the High-Capacity RNA to cDNA kit (Applied Biosystems, Foster City, CA), according to the manufacturer's instructions. TaqMan Gene Expression Assays for LC3B, glyceraldehyde-3-phosphate dehydrogenase (GAPDH), Parkin, and HCV core were purchased from Applied Biosystems, and mRNA levels were quantified in triplicate using an Applied Biosystems

7500 Real-Time PCR system, according to the supplier's recommendations. The expression value for LC3B, Parkin, and HCV core mRNA was normalized to that of GAPDH.

Statistical Analysis

Quantitative values are expressed as the means ± SD. Data were compared between the two groups using the Student's *t*-test. $P < 0.05$ was considered significant.

Results

Mitochondrial Oxidative Status *in Vitro* and *in Vivo*

After treatment with CCCP, a widely adopted reagent for inducing mitophagy, the mitochondrial membrane potential ($\Delta\Psi$) was significantly reduced irrespective of HCV infection (Figure 1A). The ratio of reduced/total glutathione content was decreased in the mitochondrial fraction after CCCP treatment in JFH1-Huh7 cells (Figure 1B). Thus, the mitochondrial oxidative status after CCCP treatment was present in HCV-infected cells (JFH1-Huh7). The ratio of reduced/total glutathione content was also decreased in the mitochondrial fraction but not in the whole liver in transgenic mice and HCV-infected chimeric mice compared with the control mice (Figure 1, C and D). These results suggest that there is a baseline oxidation level within the mitochondrial glutathione pool in these transgenic mice and HCV-infected chimeric mice. Furthermore, the mitochondria in these transgenic mice and HCV-infected chimeric mice can undergo mitophagy.

Impaired Recruitment of Parkin to the Mitochondria

Parkin phosphorylation and translocation to the mitochondria after CCCP treatment are indispensable for mitochondrial ubiquitination and subsequent autophagosome formation during the course of mitophagy.[13,15] CCCP exposure induced Parkin accumulation in the mitochondria of Huh7 cells; however, this Parkin recruitment seemed to be inhibited in JFH1-Huh7 cells (Figure 2A). CCCP treatment induces mitochondrial fission, followed by mitophagy.[13] CCCP-treated Huh7 cells displayed fragmented mitochondria colocalized with Parkin, except for a few mitochondrial tubular network cells. Western blot analysis also showed that CCCP-induced recruitment of Parkin to the mitochondria was suppressed without any change in Parkin expression or phosphorylation levels in whole cell lysates of JFH1-Huh7 cells (Figure 2B). Neither CCCP treatment nor HCV infection significantly increased the mRNA levels of Parkin in Huh7 cells, even though there was a tendency of increase in Parkin mRNA after HCV infection (Figure 2C). These results indicate that HCV infection could inhibit Parkin recruitment to CCCP-induced depolarized mitochondria.

The unique and high concentration of CCCP (10 μmol/L) used in the present study may have affected cellular functions

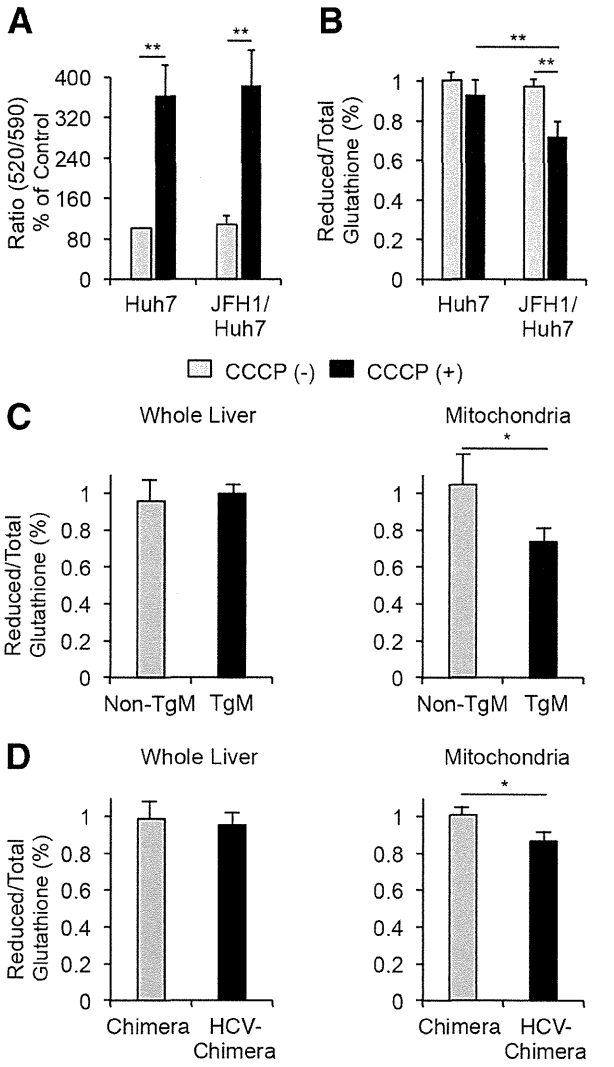

Figure 1 Mitochondrial membrane potential ($\Delta\Psi$) and glutathione content. **A:** Changes in $\Delta\Psi$ levels after a 1-hour carbonyl cyanide *m*-chlorophenylhydrazone (CCCP) treatment for Huh7 and JFH1-Huh7 cells ($n = 5$). The *y* axis represents the ratio of red (JC-10 aggregate form)/green (JC-10 monometric form) fluorescence intensity. **B:** Reduced and total glutathione content in mitochondrial fractions ($n = 5$). Reduced glutathione content was normalized to total glutathione content. Reduced and total glutathione content of freshly isolated whole liver homogenates or mitochondrial fractions of transgenic livers ($n = 7$, **C**) or HCV-infected chimeric mice livers ($n = 5$, **D**) compared with the content in the corresponding control liver samples. Reduced glutathione content was normalized to total glutathione content. $*P < 0.05$, $**P < 0.01$.

other than the proton gradient,[31] which suggests that Parkin translocation from the cytoplasm to the mitochondria may not be induced specifically through mitochondrial depolarization. Therefore, we examined mitochondrial accumulation of Parkin using lower CCCP concentrations (0.1, 1, 5, or 10 μmol/L). In coimmunoprecipitation experiments, CCCP exposure induced ubiquitinated Parkin accumulation in the mitochondria in a dose-dependent manner in Huh7 cells, as described previously,[13] but did not induce these changes in JFH1-Huh7 cells (Figure 2D). These results suggest that

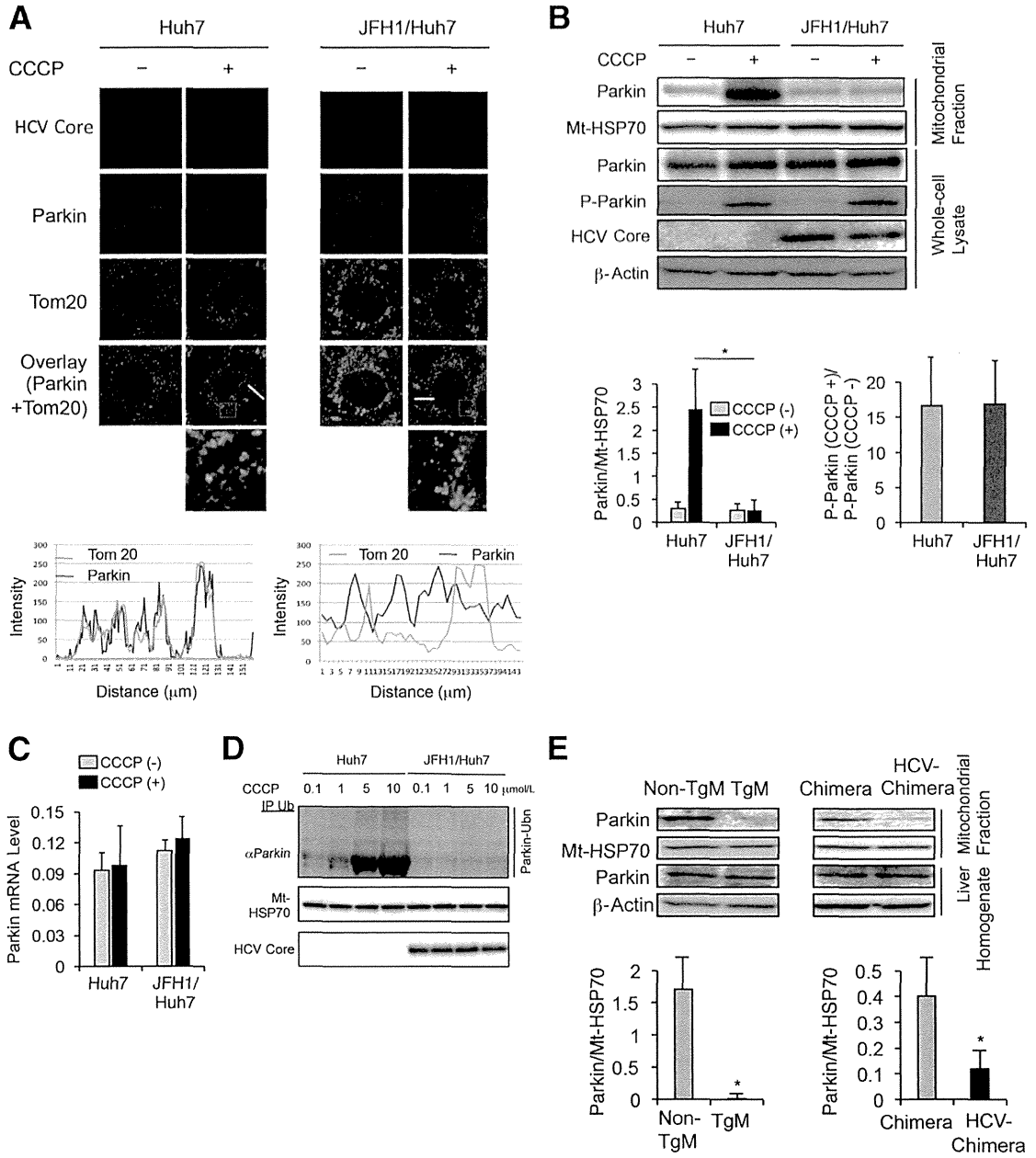

Figure 2 Effect of HCV on the translocation of Parkin to the mitochondria. **A:** Immunofluorescence staining for Parkin (red) and the mitochondrial marker Tom20 (green) in Huh7 and JFH1-Huh7 cells before (−) and after (+) carbonyl cyanide *m*-chlorophenylhydrazone (CCCP) treatment for 1 hour. **Boxed areas** are enlarged below. Endogenous Parkin that colocalizes with the mitochondria (yellow spots). Line scans indicate the colocalization of Parkin with the mitochondria and correlate to the **white lines** in the images. **Boxed areas** are enlarged below. **B:** Immunoblots for Parkin and phosphorylated Parkin (p-Parkin) using the mitochondrial fractions and whole cell lysates before and after CCCP treatment ($n = 5$). Parkin expression level was normalized to mitochondrial heat shock protein 70 (Mt-HSP70). The degree of phosphorylation was expressed as the ratio of phosphorylated Parkin after CCCP treatment to that prior treatment. **C:** Parkin mRNA level in Huh7 cells and JFH1-Huh7 cells before and after CCCP treatment ($n = 5$). The expression level for Parkin was normalized to GAPDH. **D:** Coimmunoprecipitation reveals more ubiquitinated Parkin in CCCP dose-dependent manner in Huh7 cells but not in JFH1-Huh7 cells. **E:** Immunoblots for Parkin using mitochondrial fractions of the livers or liver homogenates from non-TgM and TgM and from chimeric mice with or without HCV infection ($n = 5$ for each type of mouse). $^*P < 0.05$.

CCCP specifically induces mitophagy in Huh7 cells and that the HCV infection has an inhibitory effect on mitophagy in JFH1-Huh7 cells.

FL-N/35-transgenic mice and HCV-infected chimeric mice also showed reduced Parkin expression in the mitochondrial fraction of the liver with no change in Parkin expression levels in whole liver homogenates (Figure 2E). Serum human albumin levels, which serve as useful markers for the extent of replacement with human hepatocytes, were 16.0 ± 7.2 mg/mL in chimeric mice with HCV infection and 11.9 ± 1.7 mg/mL in chimeric mice without HCV infection (Figure 3A). These findings suggest that there was

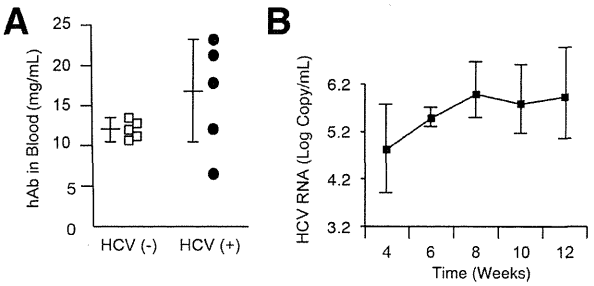

Figure 3 Human albumin and HCV RNA levels in the serum of chimeric mice with or without HCV infection. **A:** Human albumin (hAb) levels in the serum of 3-month-old chimeric mice with or without HCV infection. **B:** Serial change in HCV RNA levels in the serum after HCV infection in chimeric mice ($n = 5$).

a replacement index of >90% according to a graph of the correlation between these two parameters identified in a previous study.[25] Moreover, serum HCV RNA levels increased after infection with HCV (Figure 3B). HCV infection also suppressed the translocation of Parkin to the mitochondria in human hepatocytes.

Interaction between Parkin and the HCV Core Protein

A loss of $\Delta\Psi$ stabilizes the mitochondrial accumulation of PINK1, and PINK1 recruits Parkin from the cytoplasm to depolarized mitochondria via its kinase activity.[11–15] We confirmed that Parkin was phosphorylated to the same degree after CCCP treatment regardless of HCV infection. Therefore, we next examined the mitochondrial accumulation of PINK1. Our results indicate that PINK1 accumulated in the mitochondrial fraction after CCCP treatment, and PINK1 expression levels in whole cell lysates were comparable irrespective of HCV infection (Figure 4A). In addition, blocking PINK1 protein expression with siRNA (Figure 4B) strikingly suppressed Parkin phosphorylation (Figure 4C) and the mitochondrial Parkin signal after CCCP treatment in Huh7 cells (Figure 4D), indicating that PINK1 recruits Parkin from the cytoplasm to depolarized mitochondria via its kinase activity. Suppressed translocation of Parkin to the mitochondria by HCV infection was also confirmed after treatment with valinomycin, a K^+ ionophore that rapidly dissipates $\Delta\Psi$[32] (Figure 4E).

We next examined the association between HCV protein and Parkin and hypothesized that HCV proteins may suppress Parkin translocation to the mitochondria. Coimmunoprecipitation experiments revealed that Parkin associated with the HCV core protein but not other HCV proteins, such as NS3, NS4A, and NS5A, regardless of CCCP treatment (Figure 5A). These results suggest that the HCV core protein specifically suppressed Parkin translocation to impaired mitochondria by interacting with Parkin.

Finally, we investigated which specific Parkin domain is critical for the interaction with the HCV core protein. The proposed Parkin architecture consists of an N-terminal ubiquitin-like domain, a really interesting new gene (RING) 0 domain (RING0), and a C-terminal in-between RING domain[33] (Figure 5B). Of these domains, the RING0 domain and a complete carboxy-terminal RING configuration are critical for the translocation of Parkin to damaged mitochondria and for consequent mitophagy.[13] By using the HCV core protein as bait and either an N-terminal fragment of Parkin, including RING0 (designated Parkin 1 to 215), or a C-terminal fragment of Parkin, not including RING0 (designated Parkin 216 to 465) as prey, a Yeast Two-Hybrid assay identified a specific interaction between Parkin 1 to 215 and the HCV core protein, which was visualized as a strong blue color (activation of the *MEL1* gene encoding

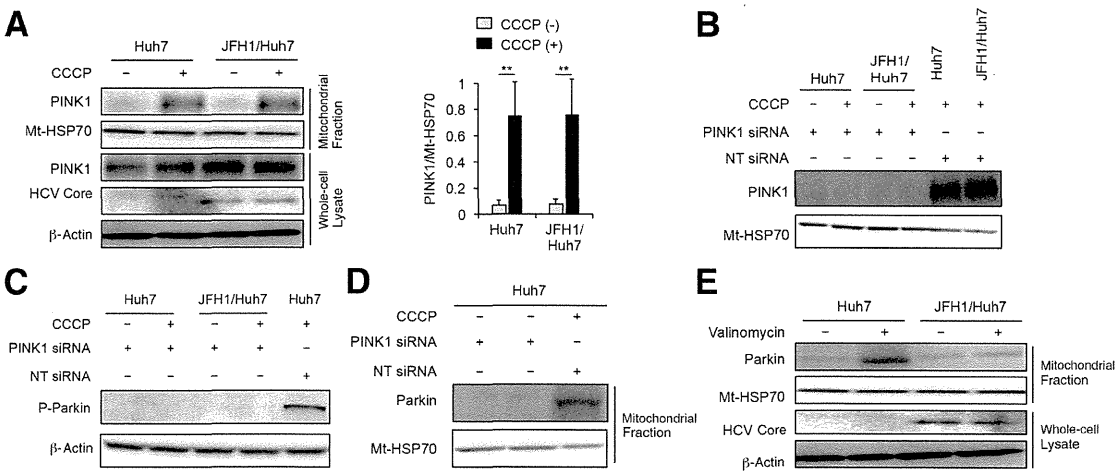

Figure 4 Mitochondrial accumulation of PINK1 after carbonyl cyanide *m*-chlorophenylhydrazone (CCCP) treatment and effect of PINK1 silencing on phosphorylation and mitochondrial translocation of Parkin. **A:** Immunoblots for PINK1 using mitochondrial fractions or whole cell lysates of Huh7 and JFH1-Huh7 cells before and after CCCP treatment ($n = 5$). Immunoblots for PINK1 using mitochondrial fractions (**B**), for phosphorylated Parkin (P-Parkin) using whole cell lysates (**C**), and for Parkin using mitochondrial fractions (**D**) of Huh7 and/or JFH1-Huh7 cells before and after CCCP treatment with or without an siRNA-mediated blockade of PINK1 expression. **E:** Immunoblots for Parkin using the mitochondrial fractions of Huh7 and JFH1-Huh7 cells before and after a 3-hour valinomycin treatment. $^{**}P < 0.01$. Mt-HSP70, mitochondrial heat shock protein 70; NT siRNA, nontargeting siRNA.

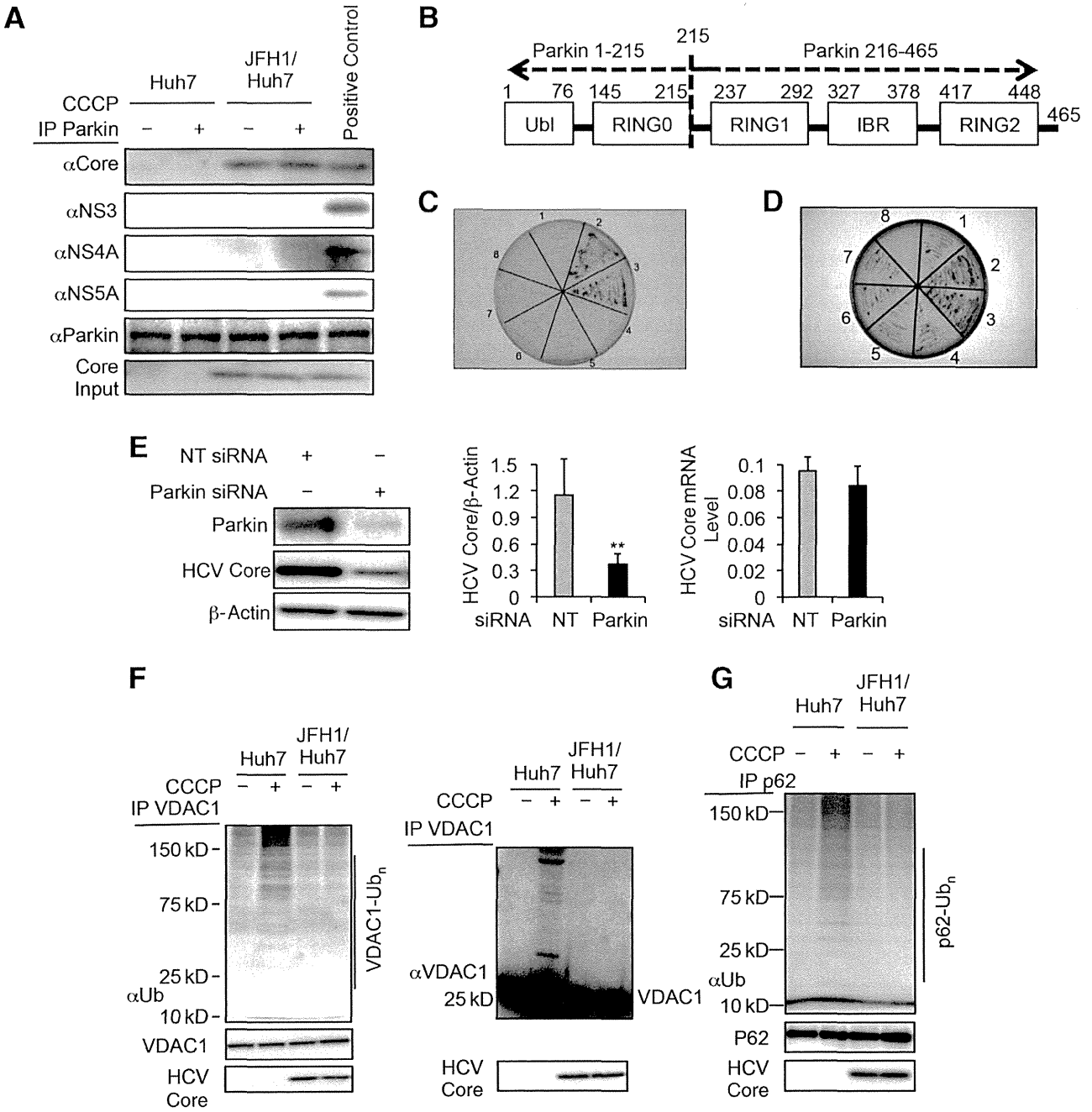

Figure 5 Interaction between Parkin and HCV core protein, effect of Parkin silencing on HCV replication, and reduction of mitochondrial outer membrane ubiquitination. **A:** Coimmunoprecipitation reveals a specific interaction of Parkin with the HCV core protein. **B:** The proposed Parkin architecture and a schematic diagram of Parkin domains. **C** and **D:** A Yeast Two-Hybrid assay identifies a specific interaction between Parkin 1 to 215 and the HCV core protein. The bait and prey for each section (1 to 8) in **C** are as follows: 1, none and none; 2, p53 and large T antigen (positive control); 3, HCV core and Parkin 1 to 215; 4, HCV core and Parkin 216 to 465; 5, HCV core and none; 6, none and Parkin 1 to 215; 7, none and Parkin 216 to 465; 8, no yeast. The bait and prey for each section in **C** were reversed in **D. E:** The HCV core protein and HCV core mRNA levels in JFH1-Huh7 cells with or without an siRNA-mediated blockade of Parkin expression ($n = 5$). **F:** Coimmunoprecipitation reveals more VDAC1 ubiquitination in Huh7 cells after carbonyl cyanide m-chlorophenylhydrazone (CCCP) treatment. Various sizes of VDAC1 immunoprecipitates are also detected by immunoblotting using an anti-VDAC1 antibody in Huh7 cells after CCCP treatment. **G:** Coimmunoprecipitation reveals more p62 ubiquitination in Huh7 cells after CCCP treatment. $^{**}P < 0.01$. IBR, in-between RING; NT, nontargeting siRNA; Parkin, Parkin-targeting siRNA; Ubl, ubiquitin-like.

α-galactosidase) (Figure 5C). In contrast, Parkin 216 to 465 did not interact with the HCV core protein. The same results were found when the core protein was used as prey and different domains of Parkin were used as bait (Figure 5D), indicating that this interaction between the two proteins was nonpolar. A previous mutational analysis of Parkin revealed that soluble Parkin mutants K211N, T240R, and G430D do not translocate to the mitochondria.[13] Although we have not

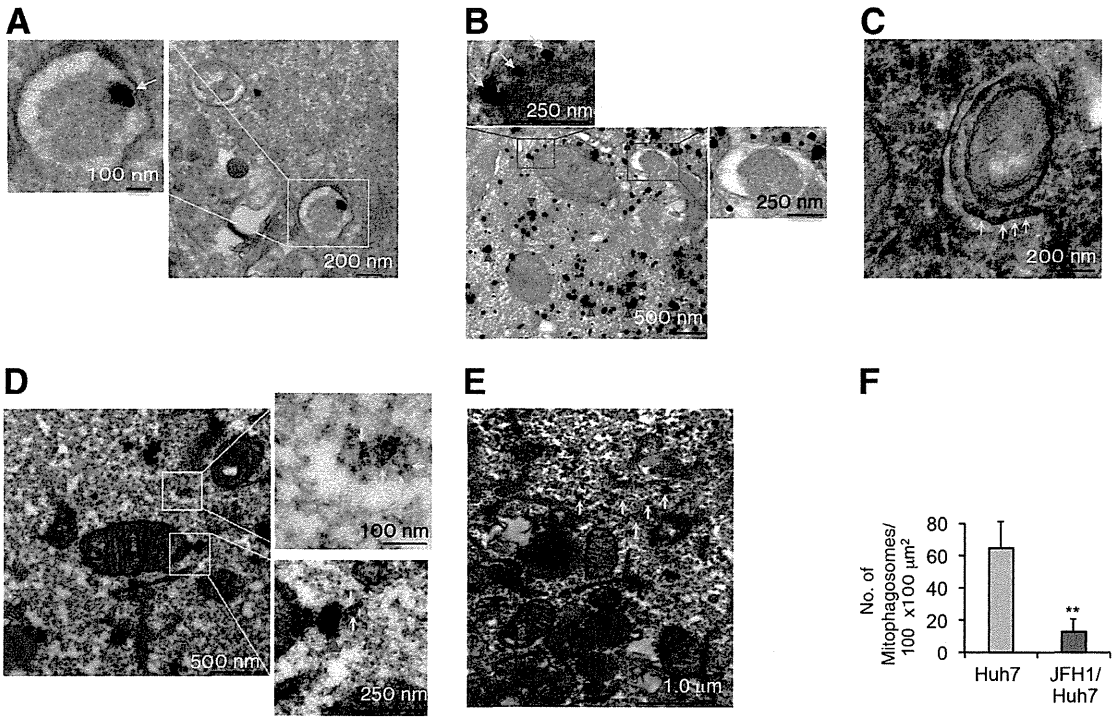

Figure 6 Electron microscopy of Huh7 cells and JFH1-Huh7 cells after carbonyl cyanide *m*-chlorophenylhydrazone (CCCP) treatment. **A—E:** Electron micrographs. **Boxed areas** are enlarged on left (Huh7 cell; **A**), above and on the right (Huh7 cell; **B**), and on the right (JFH1-Huh7 cell; **D**). The **arrows** indicate Parkin labeled with gold on the mitochondrial outer membrane (**A** and **B**), LC3 protein labeled with diaminobenzidine (DAB) on elongating isolation membrane that sequesters a single mitochondrion (Huh7 cells; **C**), Parkin core (**D**), and Parkin labeled with gold (JFH1-Huh7 cell; **E**). The **arrowheads** indicate Parkin labeled with gold (**B**) and HCV core (**D**). **F:** The number of mitophagosomes per 100 × 100 μm^2 was calculated for four randomly selected views. $^{**}P < 0.01$.

determined whether the HCV core protein binds to the region that includes lysine (K) 211 in the RING0 domain, the specific interaction of Parkin 1 to 215 with the HCV core protein raises the possibility that the core protein inhibits Parkin translocation to the mitochondria by affecting lysine 211.

After we confirmed the specific interaction between the HCV core protein and Parkin, we investigated whether Parkin affects HCV replication to investigate the functional role of the interaction between both proteins in the HCV infectious process. Parkin silencing significantly inhibited HCV replication, as indicated by a decrease in HCV core protein expression, but did not affect HCV core mRNA levels (Figure 5E). These results suggest that the association of the HCV core protein with Parkin plays a functional role in HCV propagation, although further studies are required to clarify the mechanisms.

Suppressed Ubiquitination of the Mitochondrial Outer Membrane Protein VDAC1

The next step in mitophagy after Parkin translocation to the mitochondria is the ubiquitination of mitochondrial outer membrane proteins.[13,16] Coimmunoprecipitation experiments revealed that various sizes of ubiquitinated VDAC1 species in the mitochondrial outer membrane[13] were present after CCCP treatment in Huh7 cells but not in JFH1-Huh7 cells (Figure 5F). Western blot analysis of VDAC1 immunoprecipitates revealed various sizes of VDAC1 species after CCCP treatment in Huh7 cells but not in JFH1-Huh7 cells (Figure 5F). The autophagic adaptor p62 aggregates ubiquitinated proteins by polymerizing with other p62 molecules.[13] Similarly, coimmunoprecipitation experiments revealed that CCCP treatment induced various sizes of ubiquitinated p62 species in Huh7 cells but not in JFH1-Huh7 cells (Figure 5G). These results suggest that HCV infection inhibited the Parkin-induced ubiquitination of the depolarized mitochondria.

Suppressed Mitophagosome Formation

During mitophagy, the isolation membrane sequesters a single mitochondrion or a cluster of mitochondria to form an autophagosome (mitophagosome). A single mitochondrion with Parkin on its outer membrane was sequestered by the isolation membrane after CCCP treatment in Huh7 cells (Figure 6A). Parkin in close proximity to the mitochondria and association of Parkin with mitochondrial outer membrane were observed more frequently in Huh7 cells than in JFH1-Huh7 cells (Figure 6, B, D, and E). In addition, LC3 was present on elongating isolation membrane that sequesters a single mitochondrion after CCCP treatment in Huh7 cells (Figure 6C). The number of mitophagosomes, calculated as the number of autophagosomes that contain

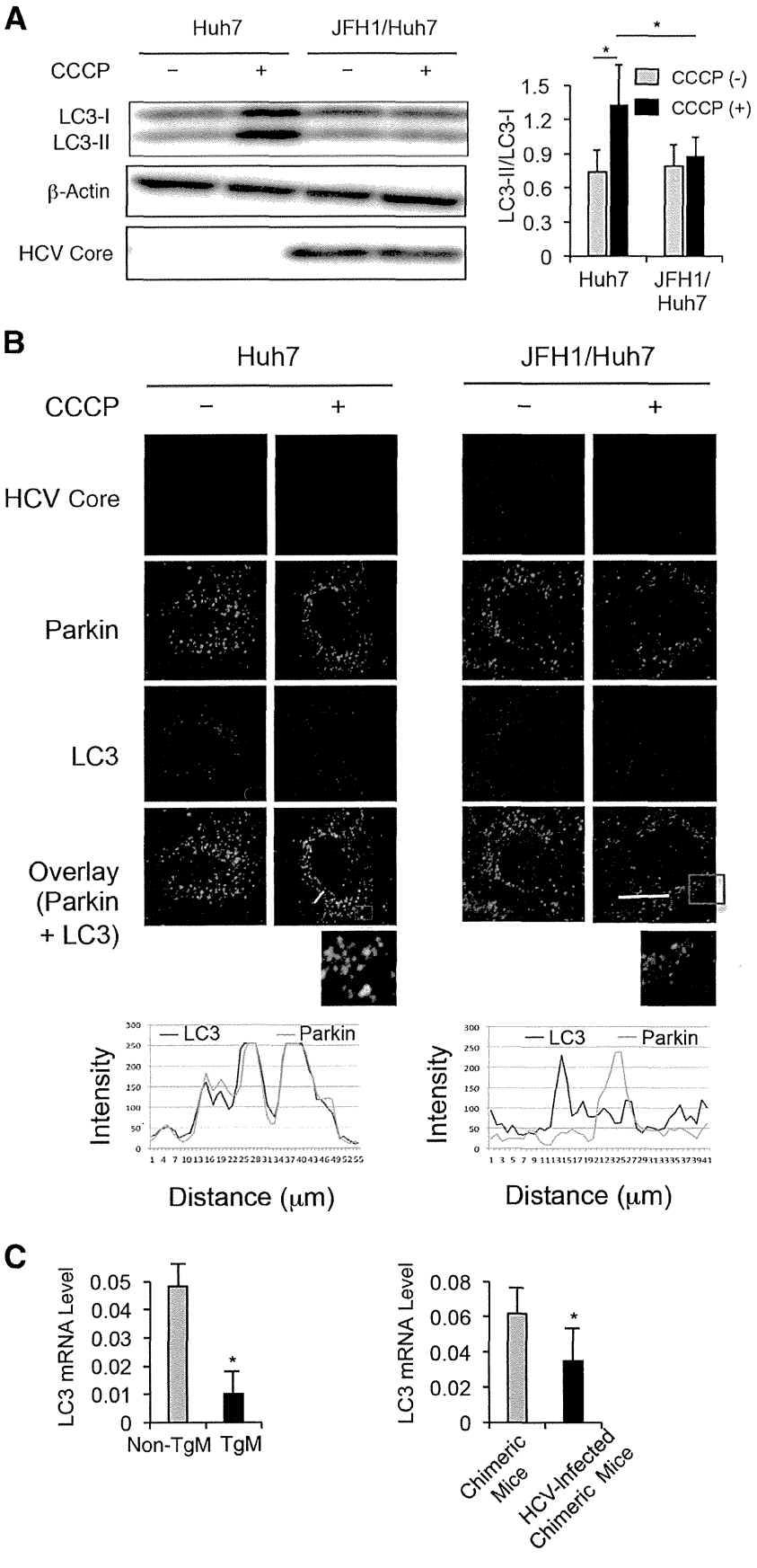

Figure 7 Effect of HCV infection on LC3-II expression and colocalization of Parkin with LC3 after carbonyl cyanide *m*-chlorophenylhydrazone (CCCP) treatment. **A:** Immunoblots for LC3-I and LC3-II using whole cell lysates of Huh7 and JFH1-Huh7 cells before and after CCCP treatment ($n = 5$). **B:** Immunofluorescence staining for Parkin (green) and LC3 (red) in Huh7 and JFH1-Huh7 cells before and after a 1-hour CCCP treatment. **Boxed areas** are enlarged below. Endogenous Parkin that colocalizes with LC3 (yellow spots). Line scans indicate the colocalization of Parkin with LC3 and correlate to the white lines in the images. **C:** The expression of LC3 mRNA in the liver from non-transgenic (non-TgM) and TgM mice ($n = 5$) and from chimeric mice without or with HCV infection ($n = 5$). The expression level of LC3 mRNA was normalized to GAPDH. $^*P < 0.05$.

mitochondria, was significantly reduced in JFH1-Huh7 cells compared with Huh7 cells (Figure 6F). Therefore, HCV infection clearly suppressed mitophagosome formation.

In agreement with suppressed mitophagosome formation, the LC3-II/I ratio was significantly lower after CCCP treatment in JFH1-Huh7 cells compared with Huh7 cells (Figure 7A), although the LC3-II/I ratio itself increased after CCCP treatment regardless of HCV infection. LC3 has been shown to be present in both complete autophagosomes and elongating isolation membranes that contain mitochondria ubiquitinated by Parkin. The present results indicate that Parkin colocalized with LC3 after CCCP treatment in Huh7 cells, whereas colocalization of Parkin and LC3 was significantly reduced in JFH1-Huh7 cells (Figure 7B). *In vivo*, FL-N/35-transgenic mice and HCV-infected chimeric mice also showed significantly reduced expression levels of LC3 mRNA in the liver compared with the control mice (Figure 7C), in agreement with reduced expression of Parkin in the mitochondrial fraction. These results may seem to be inconsistent with increased protein level of LC3-II after CCCP treatment *in vitro*. However, the lower LC3-II/I ratio after CCCP treatment in HCV-infected cells than in noninfected cells may reflect reduced expression levels of LC3 mRNA in FL-N/35-transgenic mice and HCV-infected chimeric mice. Further studies are required to clarify the mechanisms.

Several previous studies have proposed that autophagosome accumulation is enhanced on HCV infection and in HCV replicon cell lines.[34–38] Our findings of a decreased LC3-II/I ratio in JFH1-Huh7 cells, FL-N/35-transgenic mice, and HCV-infected chimeric mice seemingly contradict these previous reports. To clarify whether the decrease in LC3-II/I ratio observed in the present study indicated that macroautophagy (generally referred to as autophagy) or mitophagy was inhibited, we investigated LC3-II/I ratio in JFH1-Huh7 and Huh7 cells using Earle's balanced salt solution (EBSS) as a macroautophagy inducer (via amino acid starvation).[39] Interestingly, JFH1-Huh7 cells showed significantly increased LC3-II/I ratio compared with Huh7 cells after incubation with EBSS for 1 hour (Figure 8A), suggesting that HCV infection promoted autophagy under macroautophagy-inducible conditions. In agreement with increased LC3-II/I ratio, electron microscopy revealed that the number of autophagosomes was significantly greater after EBSS treatment in JFH1-Huh7 cells than in Huh7 cells (Figure 8B). Taken together with these results, the decrease in LC3-II/I ratio observed after CCCP treatment in JFH1-Huh7 cells likely represents a consequence of mitophagy inhibition, but not autophagy inhibition by HCV infection.

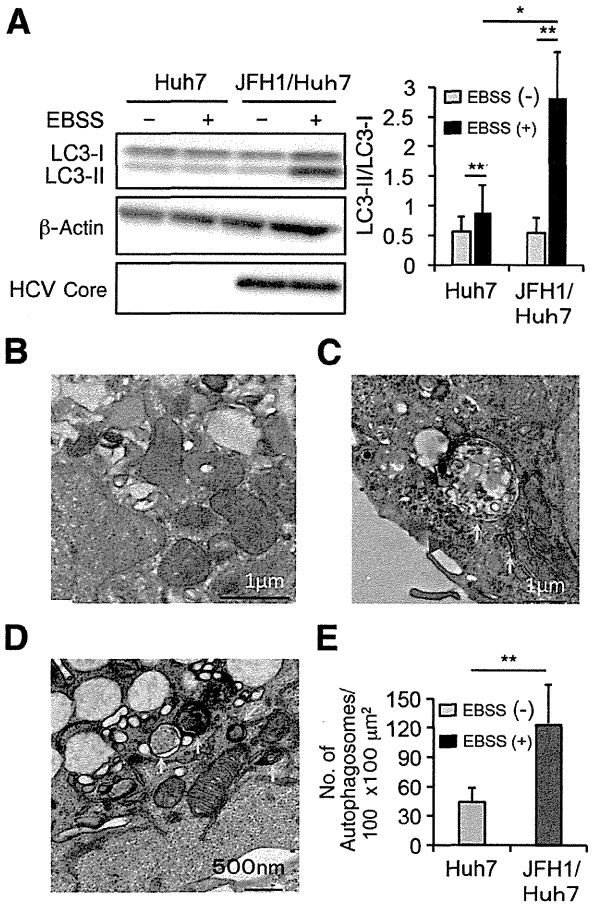

Figure 8 Effect of HCV infection on LC3-II expression and autophagosome formation after culture with Earle's balanced salt solution (EBSS). **A:** Immunoblots for LC3-II using Huh7 and JFH1-Huh7 cells before (−) and after (+) culture with EBSS ($n = 6$). The LC3-II and LC3-I expression level was normalized to β-actin. Electron microscopy of Huh7 (**B**) and JFH1-Huh7 (**C** and **D**) cells after EBSS treatment. The **arrows** indicate autophagosomes; **arrowheads**, HCV core protein. **E:** The number of autophagosomes per 100 × 100 μm² was calculated for five randomly selected views. $^{*}P < 0.05$, $^{**}P < 0.01$.

Suppression of Autophagic Degradation

The autophagic adaptor p62 can both aggregate ubiquitinated proteins by polymerizing with other p62 molecules and recruit ubiquitinated cargo into mitophagosomes by binding to LC3-II.[13] Therefore, p62 accumulation can be attributed to a deficit in autophagic degradation activity. After a 1- or 2-hour CCCP treatment, there was a smaller decrease in p62 in JFH1-Huh7 cells compared with Huh7 cells (Figure 9A). *In vivo*, FL-N/35-transgenic mice and HCV-infected chimeric mice also showed p62 accumulation in the liver compared with the control mice (Figure 9B). These results suggest that the degradation of damaged mitochondria was suppressed in the presence of HCV infection.

Finally, we assessed the change in VDAC1 content after CCCP treatment to obtain additional evidence as to whether mitophagy itself was suppressed by HCV infection. After a 2-hour CCCP treatment, a decrease in cellular content of VDAC1 was significantly smaller in JFH1-Huh7 cells than in Huh7 cells (Figure 9C). We also found that CCCP-induced increase in ROS production was greater in

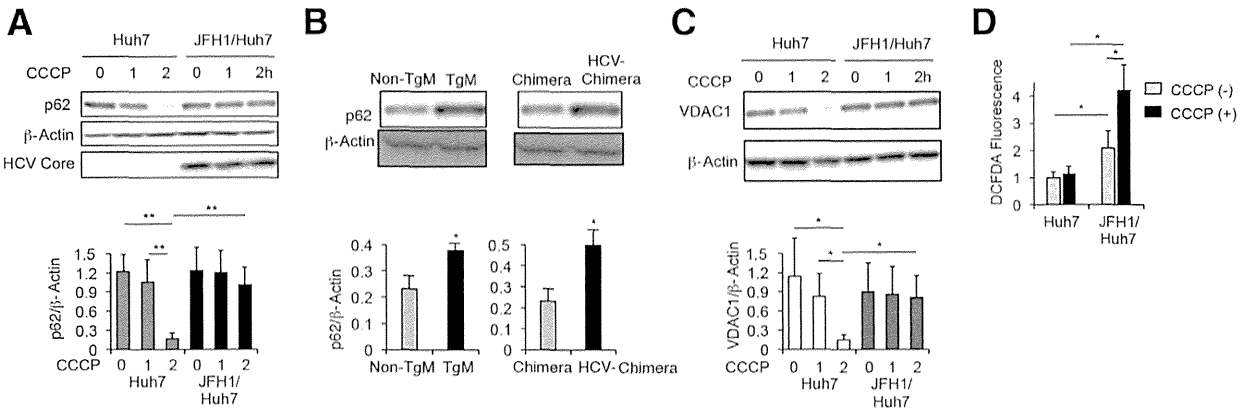

Figure 9 Effect of HCV infection on cellular p62 and VDAC1 expression after carbonyl cyanide *m*-chlorophenylhydrazone (CCCP) treatment and reactive oxygen species (ROS) production. **A:** Immunoblots for p62 using whole cell lysates of Huh7 and JFH1-Huh7 cells before and after a 1- and a 2-hour CCCP treatment ($n = 5$). **B:** Immunoblots for p62 using the liver from non-transgenic (non-TgM) and TgM ($n = 5$) mice and from chimeric mice without or with HCV infection ($n = 5$). The p62 expression level was normalized to β-actin. **C:** Immunoblots for VDAC1 using whole cell lysates of Huh7 and JFH1-Huh7 cells before and after a 1- and a 2-hour CCCP treatment ($n = 5$). The VDAC1 expression level was normalized to β-actin. **D:** Changes in cellular ROS production after a 1-hour CCCP treatment in Huh7 and JFH1-Huh7 cells ($n = 5$). $*P < 0.05$, $**P < 0.01$.

JFH1-Huh7 cells than in Huh7 cells (Figure 8D). These results were consistent with a previous study that showed an essential role of mitophagy in reducing mitochondrial ROS production[40] and, therefore, may reflect the suppressed mitophagy in the presence of HCV infection.

Discussion

Mitophagy may likely be induced in HCV-JFH1–infected cells in the context of mitochondrial depolarization, and in transgenic mice expressing the HCV polyprotein or in HCV-infected chimeric mice, both of which showed the decreased mitochondrial GSH content. Our results suggest that the HCV core protein inhibits mitophagy during HCV infection and that the molecular mechanisms by which this suppression occurs include the interaction of the HCV core protein with Parkin and the inhibition of Parkin translocation to the mitochondria. This inhibition leads to the failure of mitochondrial ubiquitination, mitophagosome formation, and autophagic degradation (Figure 10). Because Parkin 1 to 215 contains one of the critical amino acids required for mitochondrial localization, the specific interaction of Parkin 1 to 215 with the HCV core protein strongly suggests that the core protein represses mitophagy by inhibiting Parkin translocation to the mitochondria. We know that PINK1 accumulates in the mitochondria and phosphorylates Parkin after CCCP treatment and that the suppression of the mitochondrial Parkin signal occurs by blocking PINK1 via siRNA. Therefore, we could exclude the possibility that PINK1 plays a role in suppressing the recruitment of Parkin to the mitochondria. To our knowledge, this is the first report to demonstrate a suppressive effect of a viral protein on mitophagy via an interaction with Parkin. Interestingly, silencing Parkin via siRNA inhibited HCV core expression, which was consistent with the results of a recent study.[28] These results suggest that HCV potentially uses Parkin for its replication through the interaction between the HCV core protein and Parkin. Parkin may be post-transcriptionally involved in HCV replication, because Parkin silencing did not affect HCV core mRNA levels.

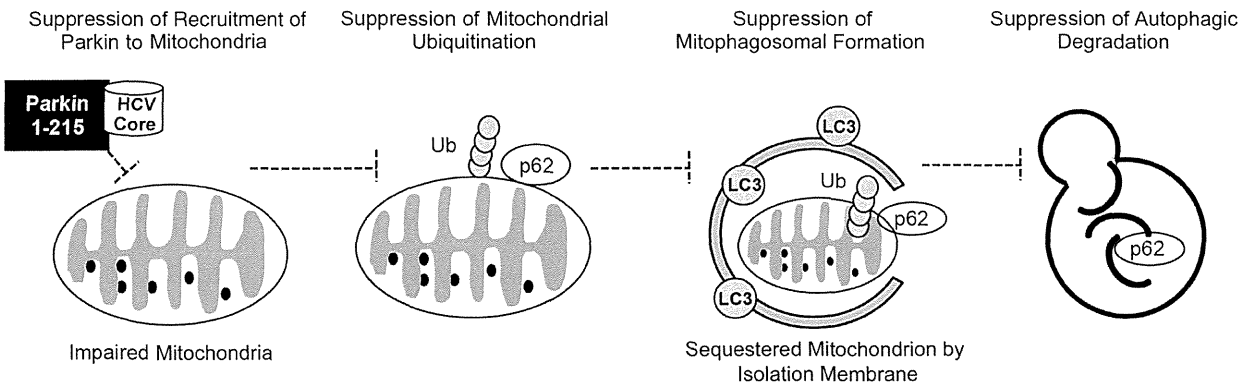

Figure 10 A schematic diagram depicting the mechanisms underlying mitophagy suppression by the HCV core protein. The HCV core protein interacts with the Parkin N-terminal fragment containing the RINGO domain (designated Parkin 1 to 215) and inhibits Parkin translocation to the mitochondria, which leads to the failure of mitochondrial ubiquitination, autophagosome formation, and autophagic degradation. Ub, ubiquitin.

Further studies are required to clarify the mechanisms underlying this speculation.

Two types of autophagy have been identified: nonselective and selective. For nonselective autophagy related to HCV infection, previous studies have reported the enhanced accumulation of autophagosomes without any effect on autophagic protein degradation,[33] the requirement of LC3 for efficient HCV replication,[34] and the occurrence of HCV RNA replication on autophagosomal membranes.[36] Mitophagy is selective and is induced by mitochondrial membrane depolarization, followed by Parkin recruitment to the mitochondria.[9–15] Herein, mitophagosome accumulation was suppressed because of mitophagy inhibition, whereas HCV infection enhanced the expression of LC3-II and autophagosome accumulation under nonselective autophagy-inducible conditions. Therefore, the present results are consistent with the previously characterized HCV-induced nonselective autophagic response.[34,35,38] However, a recent report has shown that HCV induces the mitochondrial translocation of Parkin and subsequent mitophagy,[28] which contrasts with the present results, except for the inhibitory effect of Parkin silencing on HCV replication. One of the significant differences in the method between the two studies was the presence or absence of CCCP treatment. Whether HCV-induced mitophagy was preceded by mitochondrial depolarization was unknown because $\Delta\Psi$ was not measured in the previous report of HCV-induced mitophagy.[28] However, we need to be careful that the mitochondrial depolarization by CCCP treatment is not a pathophysiological condition observed in HCV infection and that CCCP causes the depolarization of the entire mitochondrial network.[41] It is currently unknown whether CCCP treatment caused paradoxical results on mitophagy in HCV-infected cells between our study and a previous one.[28] Although suppressed mitophagy was also found in FL-N/35-transgenic mice and HCV-infected chimeric mice without any treatment, these mice may not be simply compared with HCV-JFH1–infected cells in terms of extremely low levels of viral proteins in FL-N/35-transgenic mice or spontaneous oxidized mitochondrial glutathione in both mice. Another difference between two studies was postinfection time from infection to assessment of mitophagy in HCV-JFH1–infected cells (21 versus 3 days). However, further studies are required to clarify whether postinfection time of HCV-JFH1–infected cells affects the interaction of HCV with Parkin. Oxidative stress and/or hepatocellular mitochondrial alterations are present in chronic hepatitis C to a greater degree than in other inflammatory liver diseases,[1,6] and mitophagy is important for maintaining mitochondrial quality by eliminating damaged mitochondria. Therefore, our results that the HCV core protein suppresses mitophagy appear reasonable in the context of what is known about the pathophysiological characteristics of chronic hepatitis C.

HCV-induced mitochondrial injury, ROS production, and subsequent oxidative stress contribute to HCC development in FL-N/35-transgenic mice that receive modest iron supplementation.[8] The relatively long period (12 months) required for HCC development suggests that mitochondrial injury, as a source of oxidative stress, must continue for a prolonged period. Mitochondrial DNA mutations are also relevant to HCC development in patients with chronic HCV infections.[42] Indeed, mitophagy plays an essential role in reducing mitochondrial ROS production and mitochondrial DNA mutations in yeast[40] and eliminating oxidative damaged mitochondria.[43] In addition to the directly induced generation of ROS by HCV proteins, the suppression of mitophagy by the HCV core protein has the potential to generate an additional long-lasting ROS burden and may offset or overwhelm the physiological antioxidative activity in mitochondria. Therefore, the suppressive effect of the HCV core protein on mitophagy may be an important mechanism of HCV-induced hepatocarcinogenesis.

In conclusion, results indicate that HCV core protein suppresses mitophagy by inhibiting Parkin translocation to the mitochondria via a direct interaction with Parkin in the context of mitochondrial depolarization. These findings have implications for the amplification and sustainability of mitochondria-induced oxidative stress observed in patients with HCV-related chronic liver disease and an increased risk of hepatocarcinogenesis.

Acknowledgments

We thank Dr. Stanley M. Lemon for the transgenic mice, Dr. Takaji Wakita for the JFH1 clone, and Hikari Hara for technical assistance.

References

1. Farinati F, Cardin R, De Maria N, Della Libera G, Marafin C, Lecis E, Burra P, Floreani A, Cecchetto A, Naccarato R: Iron storage, lipid peroxidation and glutathione turnover in chronic anti-HCV positive hepatitis. J Hepatol 1995, 22:449–456
2. Valgimigli M, Valgimigli L, Trere D, Gaiani S, Pedulli GF, Gramantieri L, Bolondi L: Oxidative stress EPR measurement in human liver by radical-probe technique: correlation with etiology, histology and cell proliferation. Free Radic Res 2002, 36:939–948
3. Okuda M, Li K, Beard MR, Showalter LA, Scholle F, Lemon SM, Weinman SA: Mitochondrial injury, oxidative stress, and antioxidant gene expression are induced by hepatitis C virus core protein. Gastroenterology 2002, 122:366–375
4. Moriya K, Nakagawa K, Santa T, Shintani Y, Fujie H, Miyoshi H, Tsutsumi T, Miyazawa T, Ishibashi K, Horie T, Imai K, Todoroki T, Kimura S, Koike K: Oxidative stress in the absence of inflammation in a mouse model for hepatitis C virus-associated hepatocarcinogenesis. Cancer Res 2001, 61:4365–4370
5. Korenaga M, Wang T, Li Y, Showalter LA, Chan T, Sun J, Weinman SA: Hepatitis C virus core protein inhibits mitochondrial electron transport and increases reactive oxygen species (ROS) production. J Biol Chem 2005, 280:37481–37488
6. Barbaro G, Di Lorenzo G, Asti A, Ribersani M, Belloni G, Grisorio B, Filice G, Barbarini G: Hepatocellular mitochondrial alterations in patients with chronic hepatitis C: ultrastructural and biochemical findings. Am J Gastroenterol 1999, 94:2198–2205

7. Nishina S, Hino K, Korenaga M, Vecchi C, Pietrangelo A, Mizukami Y, Furutani T, Sakai A, Okuda M, Hidaka I, Okita K, Sakaida I: Hepatitis C virus-induced reactive oxygen species raise hepatic iron level in mice by reducing hepcidin transcription. Gastroenterology 2008, 134:226–238
8. Furutani T, Hino K, Okuda M, Gondo T, Nishina S, Kitase A, Korenaga M, Xiao SY, Weinman SA, Lemon SM, Sakaida I, Okita K: Hepatic iron overload induces hepatocellular carcinoma in transgenic mice expressing the hepatitis C virus polyprotein. Gastroenterology 2006, 130:2087–2098
9. Kim I, Rodriguez-Enriquez S, Lemasters JJ: Selective degradation of mitochondria by mitophagy. Arch Biochem Biophys 2007, 462:245–253
10. Elmore SP, Qian T, Grissom S, Lemasters JJ: The mitochondrial permeability transition initiates autophagy in rat hepatocytes. FASEB J 2001, 15:2286–2287
11. Matsuda N, Sato S, Shiba K, Okatsu K, Saisho K, Gautier CA, Sou YS, Saiki S, Kawajiri S, Sato F, Kimura M, Komatsu M, Hattori N, Tanaka K: PINK1 stabilized by mitochondrial depolarization recruits Parkin to damaged mitochondria and activates latent Parkin for mitophagy. J Cell Biol 2010, 189:211–221
12. Narendra DP, Jin SM, Tanaka A, Suen DF, Gautier CA, Shen J, Cookson MR, Youle RJ: PINK1 is selectively stabilized on impaired mitochondria to activate Parkin. PLoS Biol 2010, 8:e1000298
13. Geisler S, Holmström KM, Skujat D, Fiesel FC, Rothfuss OC, Kahle PJ, Springer W: PINK1/Parkin-mediated mitophagy is dependent on VDAC1 and p62/SQSTM1. Nat Cell Biol 2010, 12:119–131
14. Vives-Bauza C, Zhou C, Huang Y, Cui M, de Vries RL, Kim J, May J, Tocilescu MA, Liu W, Ko HS, Magrane J, Moore DJ, Dawson VL, Grailhe R, Dawson TM, Li C, Tieu K, Przedborski S: PINK1-dependent recruitment of Parkin to mitochondria in mitophagy. Proc Natl Acad Sci USA 2010, 107:378–383
15. Narendra D, Tanaka A, Suen DF, Youle RJ: Parkin is recruited selectively to impaired mitochondria and promotes their autophagy. J Cell Biol 2008, 183:795–803
16. Chan NC, Salazar AM, Pham AH, Sweredoski MJ, Kolawa NJ, Graham RL, Hess S, Chan DC: Broad activation of the ubiquitin-proteasome system by Parkin is critical for mitophagy. Hum Mol Genet 2011, 20:1726–1737
17. Gegg ME, Cooper JM, Chau KY, Rojo M, Schapira AH, Taanman JW: Mitofusin 1 and mitofusin 2 are ubiquitinated in a PINK1/parkin-dependent manner upon induction of mitophagy. Hum Mol Genet 2010, 19:4861–4870
18. Chen D, Gao F, Li B, Wang H, Xu Y, Zhu C, Wang G: Parkin mono-ubiquitinates Bcl-2 and regulates autophagy. J Biol Chem 2010, 285:38214–38223
19. Narendra D, Kane LA, Hauser DN, Fearnley IM, Youle RJ: p62/SQSTM1 is required for Parkin-induced mitochondrial clustering but not mitophagy; VDAC1 is dispensable for both. Autophagy 2010, 6:1090–1106
20. Itakura E, Kishi-Itakura C, Koyama-Honda I, Mizushima N: Structures containing Atg9A and the ULK1 complex independently target depolarized mitochondria at initial stages of Parkin-mediated mitophagy. J Cell Sci 2012, 125:1488–1499
21. Okatsu K, Saisho K, Shimanuki M, Nakada K, Shitara H, Sou YS, Kimura M, Sato S, Hattori N, Komatsu M, Tanaka K, Matsuda N: p62/SQSTM1 cooperates with Parkin for perinuclear clustering of depolarized mitochondria. Genes Cells 2010, 15:887–900
22. Wakita T, Pietschmann T, Kato T, Date T, Miyamoto M, Zhao Z, Murthy K, Habermann A, Kräusslich HG, Mizokami M, Bartenschlager R, Liang TJ: Production of infectious hepatitis C virus in tissue culture from a cloned viral genome. Nat Med 2005, 11:791–796
23. Li K, Prow T, Lemon SM, Beard MR: Cellular response to conditional expression of hepatitis C virus core protein in Huh7 cultured human hepatoma cells. Hepatology 2002, 35:1237–1246
24. Lerat H, Honda M, Beard MR, Loesch K, Sun J, Yang Y, Okuda M, Gosert R, Xiao SY, Weinman SA, Lemon SM: Steatosis and liver cancer in transgenic mice expressing the structural and nonstructural proteins of hepatitis C virus. Gastroenterology 2002, 122:352–365
25. Tateno C, Yoshizane Y, Saito N, Kataoka M, Utoh R, Yamasaki C, Tachibana A, Soeno Y, Asahina K, Hino H, Asahara T, Yokoi T, Furukawa T, Yoshizato K: Near completely humanized liver in mice shows human-type metabolic responses to drugs. Am J Pathol 2004, 165:901–912
26. Kimura T, Imamura M, Hiraga N, Hatakeyama T, Miki D, Noguchi C, Mori N, Tsuge M, Takahashi S, Fujimoto Y, Iwao E, Ochi H, Abe H, Maekawa T, Arataki K, Tateno C, Yoshizato K, Wakita T, Okamoto T, Matsuura Y, Chayama K: Establishment of an infectious genotype 1b hepatitis C virus clone in human hepatocyte chimeric mice. J Gen Virol 2008, 89:2108–2113
27. Ando M, Korenaga M, Hino K, Ikeda M, Kato N, Nishina S, Hidaka I, Sakaida I: Mitochondrial electron transport inhibition in full genomic hepatitis C replicon cells is restored by reducing viral replication. Liver Int 2008, 28:1158–1166
28. Kim SJ, Syed GH, Siddiqui A: Hepatitis C virus induces the mitochondrial translocation of Parkin and subsequent mitophagy. PLoS Pathog 2013, 9:e1003285
29. Toida K, Kosaka K, Aika Y, Kosaka T: Chemically defined neuron groups and their subpopulations in the glomerular layer of the rat main olfactory bulb, IV: intraglomerular synapses of tyrosine hydroxylase-immunoreactive neurons. Neuroscience 2000, 101:11–17
30. Ikeda M, Sugiyama K, Mizutani T, Tanaka T, Tanaka K, Sekihara H, Shimotohno K, Kato N: Human hepatocyte clonal cell lines that support persistent replication of hepatitis C virus. Virus Res 1998, 56:157–167
31. Zhang GJ, Liu HW, Yang L, Zhong YG, Zheng YZ: Influence of membrane physical state on the lysosomal proton permeability. J Membr Biol 2000, 175:53–62
32. Sharpe MA, Wrigglesworth JM, Loewen J, Nicholls P: Small pH gradients inhibit cytochrome c oxidase: implications for H^+ entry to the binuclear center. Biochem Biophys Res Commun 1995, 216:931–938
33. Hristova VA, Beasley SA, Rylett RJ, Shaw GS: Identification of a novel $Zn2^+$-binding domain in the autosomal recessive juvenile Parkinson-related E3 ligase parkin. J Biol Chem 2009, 284:14978–14986
34. Sir D, Chen WL, Choi J, Wakita T, Yen TS, Ou JH: Induction of incomplete autophagic response by hepatitis C virus via the unfolded protein response. Hepatology 2008, 48:1054–1061
35. Dreux M, Gastaminza P, Wieland SF, Chisari FV: The autophagy machinery is required to initiate hepatitis C virus replication. Proc Natl Acad Sci U S A 2009, 106:14046–14051
36. Ke PY, Chen SS: Activation of the unfolded protein response and autophagy after hepatitis C virus infection suppresses innate antiviral immunity in vitro. J Clin Invest 2011, 121:37–56
37. Sir D, Kuo CF, Tian Y, Liu HM, Huang EJ, Jung JU, Machida K, Ou JH: Replication of hepatitis C virus RNA on autophagosomal membranes. J Biol Chem 2012, 287:18036–18043
38. Shrivastava S, Bhanja Chowdhury J, Steele R, Ray R, Ray RB: Hepatitis C virus upregulates Beclin1 for induction of autophagy and activates mTOR signaling. J Virol 2012, 86:8705–8712
39. Munafo DB, Colombo MI: A novel assay to study autophagy: regulation of autophagosome vacuole size by amino acid deprivation. J Cell Sci 2001, 114:3619–3629
40. Kurihara Y, Kanki T, Aoki Y, Hirota Y, Saigusa T, Uchiumi T, Kang D: Mitophagy plays an essential role in reducing mitochondrial production of reactive oxygen species and mutation of mitochondrial DNA by maintaining mitochondrial quantity and quality in yeast. J Biol Chem 2012, 287:3265–3272
41. Wang Y, Nartiss Y, Steipe B, McQibban GA, Kim PK: ROS-induced mitochondrial depolarization initiates PARK2/PARKIN-dependent mitochondrial degradation by autophagy. Autophagy 2012, 8:1462–1476
42. Nishikawa M, Nishiguchi S, Shiomi S, Tamori A, Koh N, Takeda T, Kubo S, Hirohashi K, Kinoshita H, Sato E, Inoue M: Somatic mutation of mitochondrial DNA in cancerous and noncancerous liver tissue in individuals with hepatocellular carcinoma. Cancer Res 2001, 61:1843–1845
43. Venditti P, Di Stefano L, Di Meo S: Mitochondrial metabolism of reactive oxygen species. Mitochondrion 2013, 13:71–82

Journal of General Virology (2014), **95**, 2658–2667 DOI 10.1099/vir.0.068528-0

Alternative endocytosis pathway for productive entry of hepatitis C virus

Mami Matsuda,[1] Ryosuke Suzuki,[1] Chikako Kataoka,[1] Koichi Watashi,[1] Hideki Aizaki,[1] Nobuyuki Kato,[2] Yoshiharu Matsuura,[3] Tetsuro Suzuki[4] and Takaji Wakita[1]

Correspondence
Ryosuke Suzuki
ryosuke@niid.go.jp

[1]Department of Virology II, National Institute of Infectious Diseases, Tokyo, Japan

[2]Department of Tumor Virology, Okayama University Graduate School of Medicine, Dentistry, and Pharmaceutical Sciences, Okayama, Japan

[3]Research Institute for Microbial Diseases, Osaka University, Osaka, Japan

[4]Department of Infectious Diseases, Hamamatsu University School of Medicine, Shizuoka, Japan

Previous studies have shown that hepatitis C virus (HCV) enters human hepatic cells through interaction with a series of cellular receptors, followed by clathrin-mediated, pH-dependent endocytosis. Here, we investigated the mechanisms of HCV entry into multiple HCV-permissive human hepatocyte-derived cells using trans-complemented HCV particles (HCVtcp). Knockdown of CD81 and claudin-1, or treatment with bafilomycin A1, reduced infection in Huh-7 and Huh7.5.1 cells, suggesting that HCV entered both cell types via receptor-mediated, pH-dependent endocytosis. Interestingly, knockdown of the clathrin heavy chain or dynamin-2 (Dyn2), as well as expression of the dominant-negative form of Dyn2, reduced infection of Huh-7 cells with HCVtcp, whereas infectious entry of HCVtcp into Huh7.5.1 cells was not impaired. Infection of Huh7.5.1 cells with culture-derived HCV (HCVcc) via a clathrin-independent pathway was also observed. Knockdown of caveolin-1, ADP-ribosylation factor 6 (Arf6), flotillin, p21-activated kinase 1 (PAK1) and the PAK1 effector C-terminal binding protein 1 of E1A had no inhibitory effects on HCVtcp infection into Huh7.5.1 cells, thus suggesting that the infectious entry pathway of HCV into Huh7.5.1 cells was not caveolae-mediated, or Arf6- and flotillin-mediated endocytosis and macropinocytosis, but rather may have occurred via an undefined endocytic pathway. Further analysis revealed that HCV entry was clathrin- and dynamin-dependent in ORL8c and HepCD81/miR122 cells, but productive entry of HCV was clathrin- and dynamin-independent in Hep3B/miR122 cells. Collectively, these data indicated that HCV entered different target cells through different entry routes.

Received 29 May 2014
Accepted 1 August 2014

INTRODUCTION

Over 170 million people worldwide are chronically infected with hepatitis C virus (HCV), and are at risk of developing chronic hepatitis, cirrhosis and hepatocellular carcinoma (Hoofnagle, 2002). HCV is an enveloped virus belonging to the family *Flaviviridae*. Its genome is an uncapped 9.6 kb positive-stranded RNA consisting of the 5′-UTR, an ORF encoding viral proteins and the 3′-UTR (Suzuki *et al.*, 2007). A precursor polyprotein is further processed into structural proteins (core, E1, and E2), followed by p7 and non-structural (NS) proteins (NS2, NS3, NS4A, NS4B, NS5A and NS5B), by cellular and viral proteases.

Two supplementary figures are available with the online version of this paper.

Host–virus interactions are required during the initial steps of viral infection. Viruses enter the cells by various pathways, such as receptor-mediated endocytosis followed by pH-dependent or -independent fusion from endocytic compartments, or pH-independent fusion at the plasma membrane coupled with receptor-mediated signalling and coordinated disassembly of the actin cortex (Grove & Marsh, 2011). It was reported previously that CD81 (Bartosch *et al.*, 2003; McKeating *et al.*, 2004; Pileri *et al.*, 1998), scavenger receptor class B type I (SR-BI) (Bartosch *et al.*, 2003; Scarselli *et al.*, 2002), claudin-1 (Evans *et al.*, 2007; Liu *et al.*, 2009) and occludin (Benedicto *et al.*, 2009; Liu *et al.*, 2009; Ploss *et al.*, 2009) are critical molecules for HCV entry into cells. Recently, epidermal growth factor receptor and ephrin receptor type A2 were also identified as host cofactors for HCV entry, possibly by modulating interactions between CD81 and claudin-1 (Lupberger *et al.*,

2011). In addition, Niemann–Pick C1-like 1 (NPC1L1) cholesterol absorption receptor has been shown to play a role in HCV entry, probably at the fusion step (Sainz *et al.*, 2012).

Following receptor binding, HCV has been reported to enter cultured cells via clathrin-mediated endocytosis, the most common and best-characterized mode of endocytosis, following membrane fusion in early endosomes (Blanchard *et al.*, 2006; Codran *et al.*, 2006; Coller *et al.*, 2009; Meertens *et al.*, 2006; Trotard *et al.*, 2009) using retrovirus-based HCV pseudoparticles (HCVpp) and cell culture-produced HCV (HCVcc). Early steps in HCV infection, including the role of HCV glycoprotein heterodimers, receptor binding, internalization and pH-dependent endosomal fusion, have been at least in part mimicked by HCVpp. However, as HCVpp are generated in non-hepatic cells such as human embryo kidney 293T cells, it is likely that the cell-derived component(s) of HCVpp differ from those of HCVcc.

In the present study, we readdressed the HCV endocytosis pathway using trans-complemented HCV particles (HCVtcp) (Suzuki *et al.*, 2012), of which the packaged genome is a subgenomic replicon. HCVtcp, generated in Huh-7 or its derivative cell lines with two plasmids, are infectious, but support only single-round infection, thereby allowing us to examine infectious viral entry without the influence of reinfection. In addition, HCVtcp is useful for quantifying productive infection by measuring luciferase activity. Furthermore, it has been shown that the HCVtcp system is more relevant as a model of HCV infection than HCVpp (Suzuki *et al.*, 2012). Our results demonstrated conclusively that, in addition to the clathrin-mediated endocytosis pathway, HCV was capable of utilizing the clathrin- and dynamin-independent pathways for infectious entry of HCV into human liver-derived cells.

RESULTS

HCV entry depends on receptor-mediated, pH-dependent endocytosis

HCV has been shown to enter permissive cells through clathrin-mediated endocytosis and low pH-dependent fusion with endosomes mostly using HCVpp (Codran *et al.*, 2006; Meertens *et al.*, 2006; Trotard *et al.*, 2009), although some researchers have used HCVcc with limited cell lines (Blanchard *et al.*, 2006; Coller *et al.*, 2009). However, several distinct characteristics between HCVpp and HCVcc have recently been revealed with regard to morphogenesis and entry steps (Helle *et al.*, 2010; Sainz *et al.*, 2012; Suzuki *et al.*, 2012; Vieyres *et al.*, 2010). Therefore, in this study, we used HCVtcp, which exhibit similar characteristics to HCVcc when compared with HCVpp and support single-round infection (Suzuki *et al.*, 2012).

Initially, to determine whether receptor candidates such as CD81, claudin-1, occludin and SR-BI are essential for HCV entry into Huh-7 and Huh7.5.1 cells, we examined the knockdown effect of these molecules on HCVtcp infection. Knockdown of these receptors was confirmed by immunoblotting (Fig. 1a) and FACS analysis (Fig. 1b). It should be noted that the luciferase activity in Huh7.5.1 was approximately four times higher than that in Huh-7 cells when the same amount of inoculum was used for infection (Fig. S1, available in the online Supplementary Material), and knockdown did not affect cell viability (data not shown). Knockdown of CD81 and claudin-1 significantly reduced the infection of Huh-7 and Huh7.5.1 cells with HCVtcp derived from genotype 2a (Fig. 1c). Knockdown of occludin led to a moderate reduction in infection; however, only a marginal effect was observed in SR-BI knockdown in both Huh-7 and Huh7.5.1 cells (Fig. 1c), possibly due to the reduced requirement for SR-BI during virus entry by adaptive mutation in E2 (Grove *et al.*, 2008).

Next, to examine whether HCV entry was pH-dependent, Huh-7 and Huh7.5.1 cells were pretreated with bafilomycin A1, an inhibitor of vacuolar H^+-ATPases that impairs vesicle acidification, and then infected with HCVtcp. At 72 h post-infection, luciferase activity and cell viability were determined. Bafilomycin A1 inhibited HCVtcp infection in a dose-dependent manner without affecting cell viability in both Huh-7 and Huh7.5.1 cells (Fig. 2a, b). We also confirmed that treatment with bafilomycin A1 after HCVtcp infection had a minor effect on luciferase activity (Fig. 2c). These results indicated that the infectious route of HCVtcp into Huh-7 and Huh7.5.1 cells is receptor-mediated and involves pH-dependent endocytosis.

Knockdown of clathrin heavy chain (CHC) or dynamin-2 (Dyn2) reduces HCVtcp infection in Huh-7 cells, but not in Huh7.5.1 cells

Among the known pathways of pH-dependent viral endocytosis, clathrin-mediated dynamin-dependent endocytosis is a major endocytosis pathway. Chlorpromazine, an inhibitor of clathrin-dependent endocytosis, has been commonly used to study clathrin-mediated endocytosis; however, it exerts multiple side-effects on cell function as it targets numerous receptors and intracellular enzymes, and alters plasma membrane characteristics (Sieczkarski & Whittaker, 2002a). Therefore, we examined the HCV endocytosis pathway by knockdown of specific molecules required for the endocytosis pathway. CHC, a major structural protein in clathrin-coated vesicles, and Dyn2, a GTPase essential for clathrin-coated-pit scission from the plasma membrane, play important roles in the clathrin-mediated pathway. Another well-studied model of viral entry is caveolin-mediated endocytosis. The role of dynamin in both clathrin-mediated endocytosis and caveolae-dependent endocytosis has been established (Marsh & Helenius, 2006; Miaczynska & Stenmark, 2008). To examine the endocytosis pathways of HCV, small interfering RNAs (siRNAs) for CHC, Dyn2 and caveolin-1 (Cav1), or scrambled control siRNA, were transfected into Huh-7 or

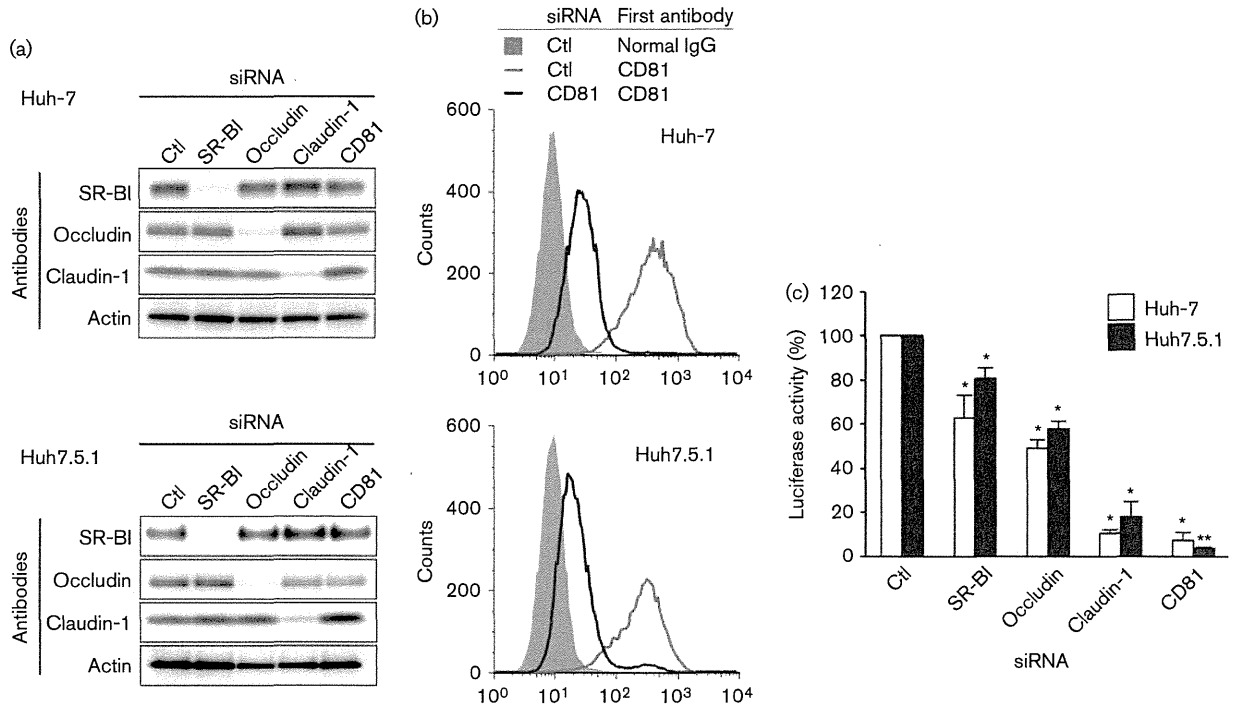

Fig. 1. Knockdown effect of receptor candidate molecules on HCV infection. (a) Huh-7 or Huh7.5.1 cells were transfected with the indicated small interfering RNAs (siRNA), harvested at 48 h post-transfection and the specific knockdown of each protein was verified by immunoblotting. (b) Huh-7 or Huh7.5.1 cells were transfected with CD81 or control siRNAs, harvested at 48 h post-transfection and the cell surface expression of CD81 was verified by FACS analysis. (c) Cells transfected with siRNA were infected with the same amount of HCVtcp at 48 h post-transfection. Firefly luciferase activity in the cells was determined at 72 h post-infection and is expressed relative to the activity with control siRNA transfection. The value for control (Ctl) siRNA was set at 100 %. Data represent the mean ± SD. Statistical differences between controls and each siRNA were evaluated using Student's *t*-test. **P*<0.05, ***P*<0.001 versus control.

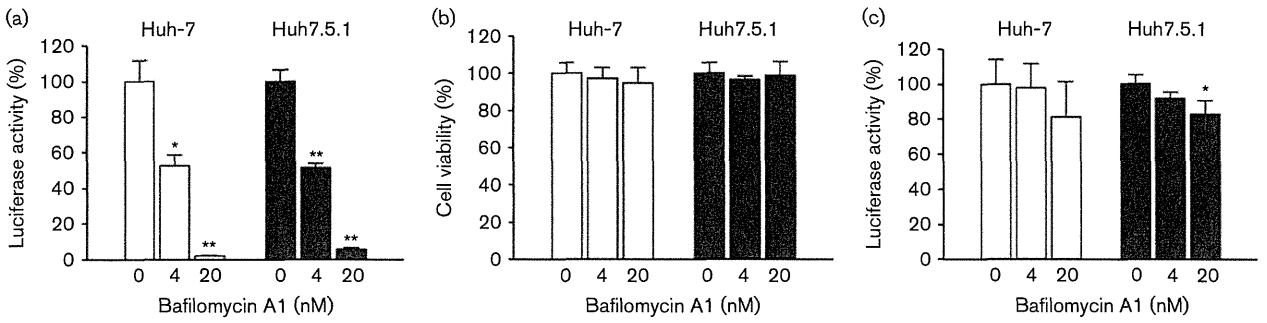

Fig. 2. Role of endosomal low pH in HCV infection. Cells were treated with bafilomycin A1 for 1 h at the indicated concentrations and infected with HCVtcp. (a, b) Luciferase activity (a) and cell viability (b) were determined at 72 h post-infection, and expressed relative to amounts observed in controls. (c) Cells were treated with bafilomycin A1 for 1 h at the indicated concentrations 48 h after HCVtcp infection. Luciferase activity was determined at 10 h post-treatment and expressed relative to amounts observed in controls. Data represent the mean ± SD. Statistical differences between controls and indicated concentrations were evaluated using Student's *t*-test. **P*<0.05, ***P*<0.001 versus control.

Huh7.5.1 cells, followed by infection with HCVtcp. Expression of CHC, Dyn2 and Cav1 was downregulated by transfection of specific siRNAs (Fig. 3a, b), whereas expression of SR-BI, occludin, claudin-1 and CD81 was not reduced (Figs 3a and S2). As indicated in Fig. 3(c), luciferase activity from HCVtcp was significantly reduced by knockdown of CHC and Dyn2 in Huh-7 cells, but not in Huh7.5.1 cells. Knockdown of Cav1 showed no inhibitory effects on HCVtcp entry into either cell line. Dynamin-independent entry in Huh7.5.1 cells was also observed using HCVtcp derived from genotype 1b (data not shown). Knockdown of CHC or Dyn2 also reduced entry of HCVcc in Huh-7 cells, but had no inhibitory effects in Huh7.5.1 (Fig. 3d). To rule out the possibility of effects on CHC and Dyn2 knockdown on viral RNA replication, HCVtcp were also inoculated before siRNA transfection. Luciferase activity was not affected by knockdown of CHC or Dyn2 in either cell line, whereas marked inhibition was observed for phosphatidylinositol 4-kinase (PI4K) (Fig. 3e). These data suggested that HCV entry was clathrin-mediated and dynamin-dependent in Huh-7 cells, but productive entry of HCV was clathrin- and dynamin-independent in Huh7.5.1 cells.

Expression of the dominant-negative form of Dyn2 reduces HCV infection in Huh-7 cells, but not in Huh7.5.1 cells

We also examined the role of dynamin in infectious entry of HCV into Huh-7 and Huh7.5.1 cells by overexpression of the dominant-negative form of Dyn2 (Dyn-K44A), which

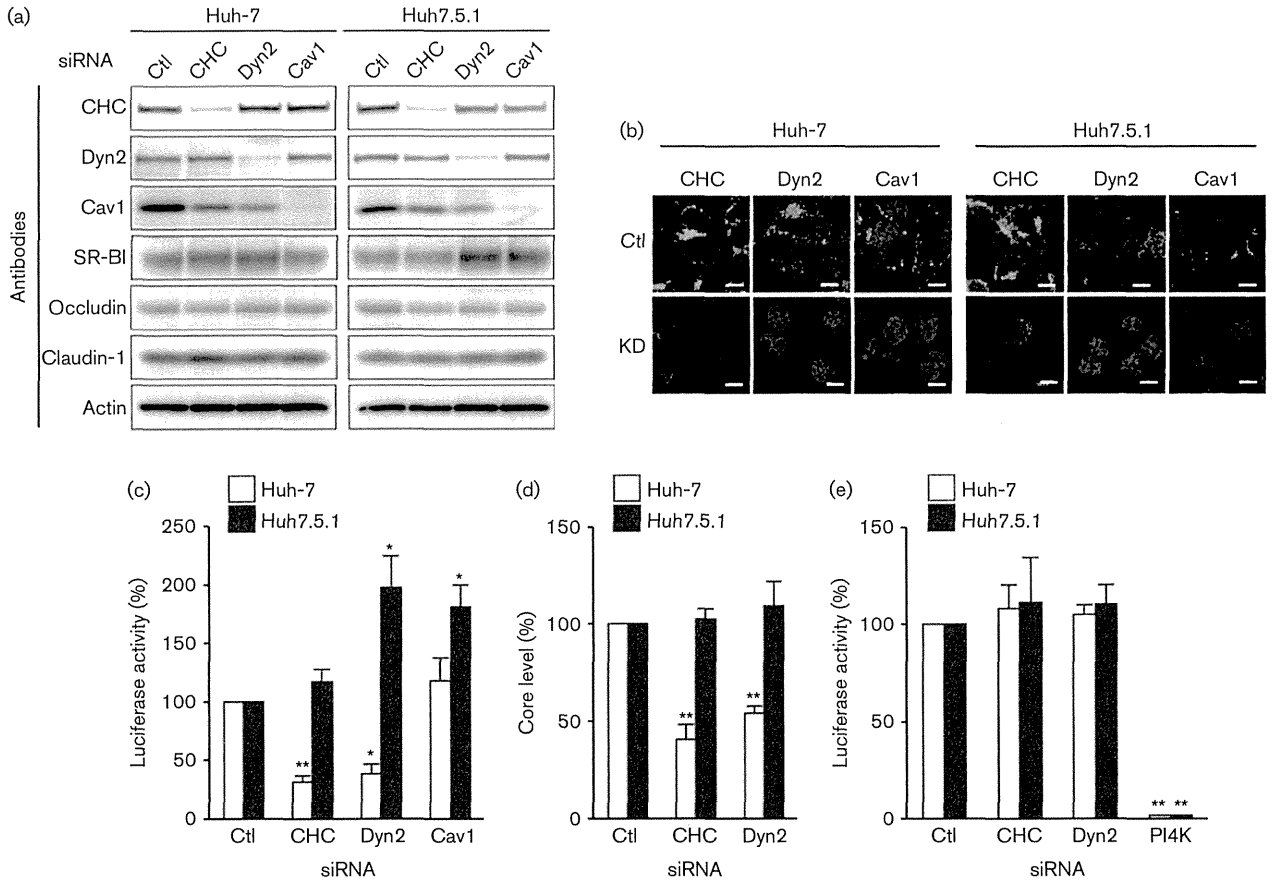

Fig. 3. Effects of CHC, Dyn2 and Cav1 knockdown on HCV infection. (a, b) Huh-7 cells or Huh7.5.1 cells were transfected with the indicated siRNAs and the specific knockdown (KD) of each protein was verified by immunoblotting (a) or immunostaining (b) at 48 h post-transfection. Bar, 50 μm. (c) Cells were transfected with the indicated siRNAs, followed by infection with HCVtcp at 48 h post-transfection. Firefly luciferase activity in the cells was subsequently determined at 3 days post-infection. The value for control (Ctl) siRNA was set at 100 %. Data represent the mean ± SD. (d) Cells were transfected with siRNA, followed by infection with HCVcc at 48 h post-transfection. Intracellular core levels were quantified at 24 h post-infection. The value for control siRNA was set at 100 %. Data represent the mean ± SD. (e) Cells were infected with HCVtcp, followed by transfection with the indicated siRNAs. Luciferase activity in the cells was subsequently determined at 2 days post-transfection. The value for control siRNA was set at 100 %. Data represent the mean ± SD. Statistical differences between controls and each siRNA were evaluated using Student's *t*-test. $^{*}P<0.05$, $^{**}P<0.001$ versus control.

has been shown to effectively block clathrin-dependent and caveolar endocytosis (Damke *et al.*, 1995). Expression of haemagglutinin (HA)-tagged Dyn-K44A reduced the number of HCV-infected Huh-7 cells, but not Huh7.5.1 cells, as compared with WT HA-tagged Dyn2 (Dyn-WT), as shown in Fig. 4(a, b). Interestingly, internalization of transferrin, which is known to be mediated by clathrin-dependent endocytosis, was reduced in both Huh-7 and Huh7.5.1 cells expressing Dyn-K44A, whereas cells expressing Dyn-WT showed efficient endocytosis of transferrin (Fig. 4c, d). Collectively, these results suggested that dynamin participated in the internalization of HCV in Huh-7 cells, but was not absolutely required in Huh7.5.1 cells, although transferrin was taken up via dynamin-dependent endocytosis in both Huh-7 and Huh7.5.1 cells.

Flotillin-1 or the GTPase regulator associated with focal adhesion kinase 1 (GRAF1) play no major role during HCV infection of Huh7.5.1 cells

In order to dissect the major endocytosis pathways of HCVtcp in Huh7.5.1 cells, we investigated the role of alternative routes of HCV entry by siRNA knockdown. We silenced essential factors for the clathrin- or dynamin-independent pathways

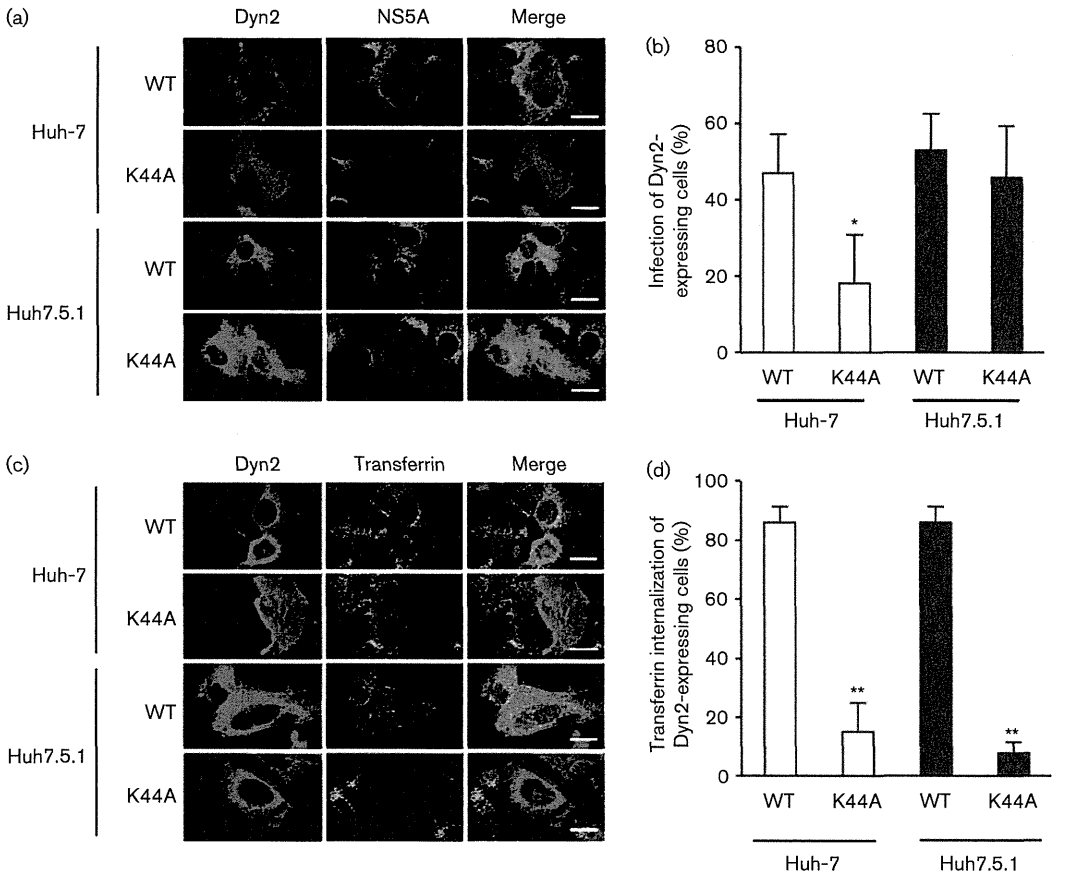

Fig. 4. Dynamin participates in the internalization of HCV in Huh-7 cells, but not in Huh7.5.1 cells. (a) Cells were transfected with HA-tagged WT Dyn2 (Dyn-WT) or dominant-negative Dyn2 (Dyn-K44A) expression plasmids. At 2 days post-transfection, cells were infected with HCVtcp, which possessed a subgenomic replicon without the luciferase gene. After 3 days, cells were fixed and HA-Dyn2 or HCV NS5A stained with anti-HA or anti-NS5A antibodies, respectively. Cell nuclei were counterstained with DAPI. Bar, 100 μm. (b) Data were quantified as the population of HCVtcp-infected cells among HA-positive cells. At least 20 HA-positive cells were evaluated in triplicate experiments. Data represent the mean ± SD. (c) Cells were transfected with HA-tagged Dyn-WT or Dyn-K44A expression plasmids. At 2 days post-transfection, cells were incubated with Alexa Fluor-488 labelled transferrin at 37 °C in a 5 % CO_2 incubator. After 30 min of incubation, cells were washed, fixed and stained with anti-HA antibodies. Cell nuclei were counterstained with DAPI. Bar, 100 μm. (d) Data were quantified as the population of transferrin-internalized cells among HA-positive cells. At least 20 HA-positive cells were evaluated in triplicate experiments. Data represent the mean ± SD. Statistical differences between Dyn-WT and Dyn-K44A were evaluated using Student's *t*-test. **P*<0.05, ***P*<0.001 versus Dyn-WT.

including flotillin-dependent endocytosis, ADP-ribosylation factor 6 (Arf6)-dependent endocytosis, clathrin-independent carrier/glycosylphosphatidylinositol-enriched early endosomal compartment (CLIC/GEEC) endocytic pathway and macropinocytosis in Huh7.5.1 cells. Flotillin-1 and Arf6 are indispensable components of the flotillin and Arf6 pathways, respectively. Knockdown of flotillin-1 or Arf6 had no inhibitory effects on HCVtcp infection in Huh7.5.1 cells (Fig. 5a). The CLIC/GEEC endocytic pathway has recently become better defined and is regulated by the GTPase regulator associated with focal adhesion kinase-1 (GRAF1). However, GRAF1 was not detected in Huh-7 or Huh7.5.1 cells (Fig. 5b); thus, it is unlikely that the CLIC/GEEC pathway was involved in HCV entry in Huh7.5.1 cells. In addition, knockdown of p21-activated kinase 1 (PAK1) and the PAK1 effector C-terminal binding protein 1 of E1A (CtBP1), which play important regulatory roles in the process of macropinocytosis, did not inhibit HCVtcp infection in Huh7.5.1 cells (Fig. 5c). Taken together, these results suggested that the entry of HCVtcp into Huh7.5.1 cells was not mediated mainly by flotillin-dependent endocytosis, Arf6-dependent endocytosis, the CLIC/GEEC endocytic pathway and macropinocytosis.

Clathrin-dependent and -independent pathways for HCV entry in other hepatic cells

We further examined the endocytosis pathways for HCV in non-Huh-7-related human liver-derived cell lines. Three HCVcc permissive hepatocellular carcinoma cell lines, Li23-derived ORL8c (Kato *et al.*, 2009), HepCD81/miR122 cells (HepG2/CD81 cells overexpressing miR122) and Hep3B/miR122 (Kambara *et al.*, 2012), were transfected with siRNA for CHC, Dyn2 or claudin-1, followed by infection with HCVtcp. Immunoblotting was performed in order to confirm knockdown of target proteins (Fig. 6a). Although knockdown of CHC or Dyn2 expression inhibited HCVtcp infection of ORL8c and HepCD81/miR122 cells, HCVtcp infection of Hep3B/miR122 cells was not affected (Fig. 6b), thus suggesting that productive entry of HCV is clathrin- and dynamin-independent in Hep3B/miR122 cells.

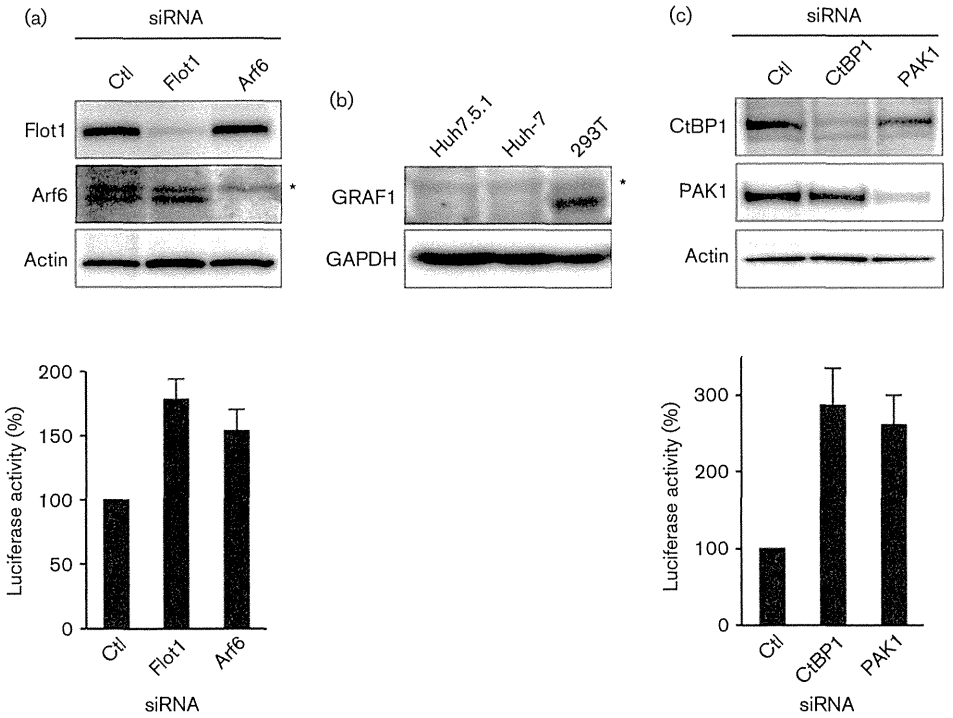

Fig. 5. Role of an alternative endocytosis pathway of HCV in Huh7.5.1 cells. (a) Huh7.5.1 cells were transfected with flotillin-1 (Flot1) or Arf6 siRNAs and specific knockdown of each protein was verified by immunoblotting (upper). Non-specific bands are marked with an asterisk. Cells transfected with siRNA were infected with HCVtcp. Luciferase activity (lower) was determined at 72 h post-infection and expressed relative to the amount observed in control (Ctl) siRNA transfection, Data represent the mean ± SD. (b) Expression of GRAF1 and glyceraldehyde 3-phosphate dehydrogenase (GAPDH) in Huh7.5.1, Huh-7 and 293T cells was analysed by immunoblotting. Non-specific bands are marked with an asterisk. (c) Huh7.5.1 cells were transfected with CtBP1 or PAK1 siRNA and specific knockdown of each protein was verified by immunoblotting (upper). Cells transfected with siRNA were infected with the HCVtcp. Luciferase activity (lower) was determined at 72 h post-infection and expressed relative to the amount observed in control (Ctl) siRNA transfection. Data represent the mean ± SD.

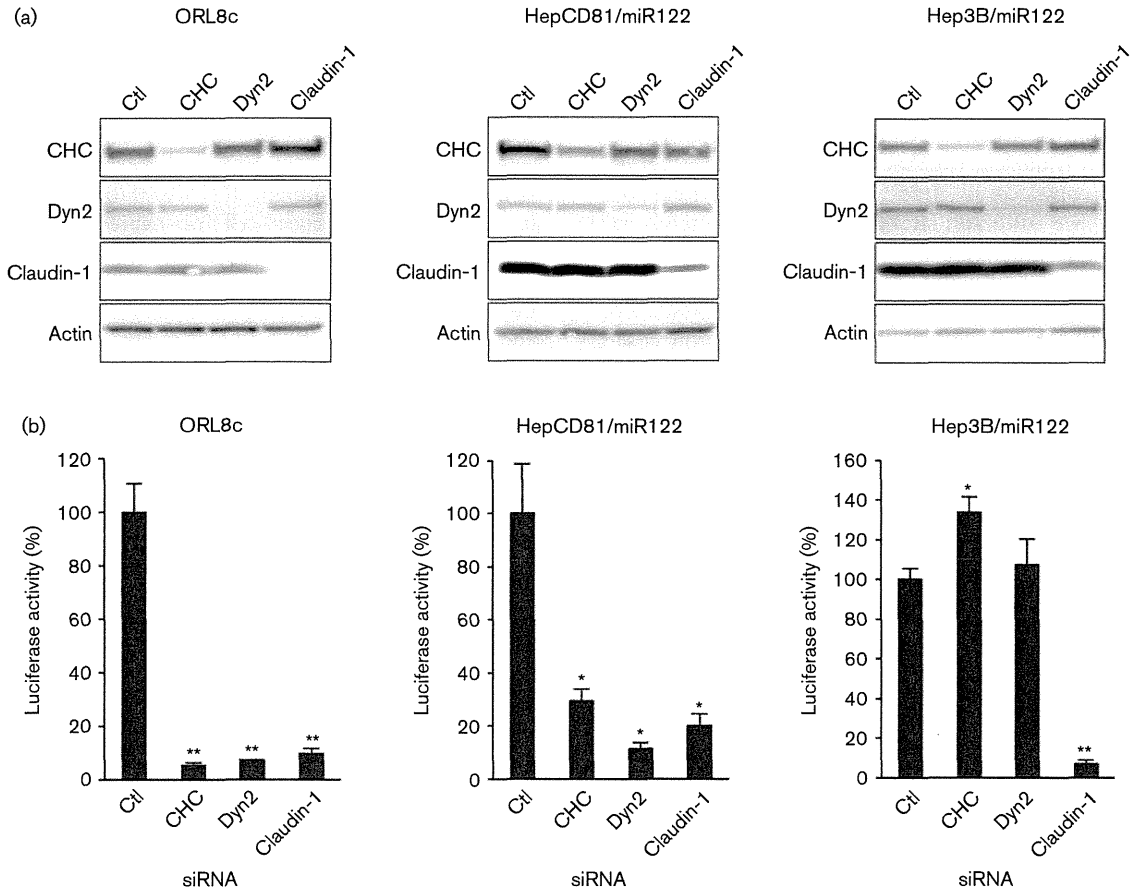

Fig. 6. Clathrin-dependent and -independent pathway of HCV entry in other HCV-permissive cells. The indicated cells were transfected with the indicated siRNAs and then infected with HCVtcp at 48 h post-transfection. (a) Specific knockdown of each protein was verified by immunoblotting. (b) Luciferase activity was determined at 72 h post-infection and expressed relative to the amount observed in the control (Ctl) siRNA transfection. Data represent the mean ± SD. Statistical differences between controls and each siRNA were evaluated using Student's *t*-test. **P*<0.05, ***P*<0.001 versus control.

In summary, we identified an alternative clathrin- and dynamin-independent entry pathway for HCV in at least two independent cell lines, Huh7.5.1 and Hep3B/miR122 cells, in addition to the previously reported clathrin- and dynamin-dependent pathway. These findings provided clues for understanding the molecular mechanisms of the endocytosis pathway for HCV infection.

DISCUSSION

Many viruses have been shown to utilize a number of different endocytic pathways to productively infect their hosts. Clathrin-dependent endocytosis would appear to be the most commonly used, but it is increasingly clear that a number of clathrin-independent endocytosis pathways are also used by several different viruses (Mercer *et al.*, 2010). In the case of HCV, it has been reported that viral entry is mediated by clathrin-dependent endocytosis (Blanchard *et al.*, 2006; Codran *et al.*, 2006; Coller *et al.*, 2009; Meertens *et al.*, 2006; Trotard *et al.*, 2009). In these papers, HCVpp was used at least in part for analysis of HCV entry pathway. However, recent reports have revealed several different characteristics between HCVpp and HCVcc.

Viral entry has been addressed primarily by pharmacologic inhibitor studies, immunofluorescence and electron microscopy, by transfection with dominant-negative constructs, and more recently by siRNA knockdown. Analysis of endocytosis pathways using pharmacological inhibitors has raised concerns about specificity. For example, chlorpromazine, an inhibitor of clathrin-mediated endocytosis, has been shown to exert multiple side-effects on cell function as it targets numerous receptors and intracellular enzymes, and alters plasma membrane characteristics (Sieczkarski & Whittaker, 2002a). Methods for elucidating the viral endocytosis pathway by co-localization of virus particles with host factor also have limitations. Electron and

fluorescence microscopy, which require a high particle number, do not allow the differentiation of infectious and non-infectious particles. Infectious particles of HCV in the supernatant of infected cells appeared to represent only a small portion of secreted virus particles (Akazawa *et al.*, 2008) and it is unclear whether the viral particles observed by microscopy could lead to productive infection. Therefore, we utilized HCVtcp, which is useful for determining productive entry of the virus without reinfection, and a combination of siRNA knockdown and dominant-negative mutants for analysis of the productive route of infection. Although HCVcc is also utilized in analysis of productive entry, it cannot completely exclude the effects of reinfection by virus produced by infected cells. Reduction of HCVcc infection by knockdown of CHC and Dyn2 was moderate when compared with that of HCVtcp (Fig. 3c, d), thus suggesting slight effects due to reinfection in HCVcc.

The data presented here demonstrate for the first time to our knowledge that HCV is able to enter cells via dynamin-independent endocytosis in addition to the previously described classical clathrin- and dynamin-dependent pathway. First, knockdown of CHC and Dyn2 had no inhibitory effects on HCVtcp and HCVcc entry into Huh7.5.1 cells. Second, overexpression of dominant-negative Dyn2 had no inhibitory effects on HCVtcp in Huh7.5.1 cells. Finally, in addition to Huh7.5.1 cells, Hep3B/miR122 cells were also shown to be infected with HCV via clathrin- and dynamin-independent pathways. We further investigated the role of alternative minor routes of HCV entry into Huh7.5.1 cells; however, the productive endocytosis pathway could not be defined. It should be noted that inhibition of alternative endocytosis routes by siRNA led to an increase of luciferase activity (Figs 3c and 5a, c). This could be explained by the inhibition of a particular endocytosis pathway resulting in a compensatory increase in alternative endocytosis pathways (Damke *et al.*, 1995).

Although we confirmed an alternative endocytosis pathway for the productive entry of HCV, it is not clear why and how the two independent endocytosis pathways operate in different cell lines. SV40 can enter cells via caveolae-dependent (Norkin *et al.*, 2002; Pelkmans *et al.*, 2001) and -independent (Damm *et al.*, 2005) pathways. Influenza virus enters cells via clathrin-mediated endocytosis (Matlin *et al.*, 1981) in addition to non-clathrin-mediated, non-caveola-mediated internalization pathways (Sieczkarski & Whittaker, 2002b). Entry of dengue virus type 2 is clathrin-dependent in HeLa and C6/36 cells (Acosta *et al.*, 2008; Mosso *et al.*, 2008; van der Schaar *et al.*, 2008), and is clathrin-independent in Vero cells (Acosta *et al.*, 2009). Different receptor usage may determine the consequential route of entry. However, we did not observe any differences between Huh-7 and Huh7.5.1 cells in terms of knockdown effects of receptor candidate molecules on HCV infection, as shown in Fig. 1(c), although we cannot exclude the possibility that other undefined receptors are associated with viral entry. Huh7.5.1 cells were established by elimination of the HCV genome from replicon cells derived from Huh-7 cells (Blight *et al.*, 2002; Zhong *et al.*, 2005) and they exhibit more potent replication of HCV than the original Huh-7 cells. Further study showed that the increased permissiveness of cured cells results from a mutation in the retinoic acid-inducible gene I (Sumpter *et al.*, 2005), which impairs IFN signalling. In addition, it has been shown that cured cell lines express higher levels of miR122 than parental cells participating in the efficient propagation of HCVcc (Kambara *et al.*, 2012). As it is unclear whether these changes are the reason for a distinct endocytosis pathway, it will be of interest to explore these associations in further studies.

In conclusion, we confirmed an alternative clathrin-independent endocytosis pathway in HCV-permissive human hepatic-derived cells, in addition to the previously reported clathrin-dependent endocytosis pathway. This paper highlights the fact that clathrin- and dynamin-mediated endocytosis is the main route of HCV entry for Huh-7, HepCD81/miR122 and ORL8c cells, whilst clathrin and dynamin do not play a major role during the productive route of HCV infection in Huh7.5.1 and Hep3B/miR122 cells. Taken together, these studies suggest that different cell entry pathways for HCV infection may be utilized in different cell types, although further studies are necessary in order to understand this phenomenon.

METHODS

Cells. The human hepatocellular carcinoma cell lines Huh-7, Huh7.5.1, Hep3B/miR122 and HepG2/CD81, which overexpressed miR122 (Kambara *et al.*, 2012), were maintained in Dulbecco's modified Eagle's medium (DMEM; Wako Pure Chemical Industries) containing non-essential amino acids, penicillin (100 U ml^{-1}), streptomycin (100 μg ml^{-1}) and 10 % FBS. Li23-derived ORL8c cells (Kato *et al.*, 2009) were maintained in F12 medium and DMEM (1 : 1, v/v) supplemented with 1 % FBS, epidermal growth factor (50 ng ml^{-1}), insulin (10 μg ml^{-1}), hydrocortisone (0.36 μg ml^{-1}), transferrin (5 μg ml^{-1}), linoleic acid (5 μg ml^{-1}), selenium (20 ng ml^{-1}), prolactin (10 ng ml^{-1}), gentamicin (10 μg ml^{-1}), kanamycin monosulfate (0.2 mg ml^{-1}) and fungizone (0.5 μg ml^{-1}). All cell lines were cultured at 37 °C in a 5 % CO_2 incubator.

Preparation of viruses. HCVtcp and HCVcc derived from JFH-1 with adaptive mutations in E2 (N417S), p7 (N765D) and NS2 (Q1012R) were generated as described previously (Suzuki *et al.*, 2012). For HepCD81/miR122 and ORL8c cells, HCVtcp containing the *Gaussia* luciferase (GLuc) reporter gene were used. To do this, plasmid pHH/SGR-JFH1/GLuc/NS3m carrying the bicistronic subgenomic HCV replicon containing the GLuc reporter gene and the NS3 adaptive mutation was constructed by replacement of the firefly luciferase (FLuc) gene of pHH/SGR-Luc containing the NS3 mutation (N1586D) (Suzuki *et al.*, 2012) with the GLuc gene of pCMV-GLuc (NEB).

Plasmids. HA-tagged Dyn2, a dominant-negative Dyn2 (K44A) in which Lys44 was replaced with Ala, was cloned into pcDNA3.1 as described previously (Kataoka *et al.*, 2012).

Gene silencing by siRNA. siRNAs were purchased from Sigma-Aldrich and were introduced into the cells at a final concentration of